Stau coannihilation, compressed spectrum, and SUSY discovery potential at the LHC

Amin Aboubrahim, Pran Nath, and Andrew B. Spisak

Phys. Rev. D **95**, 115030 — Published 26 June 2017

DOI: 10.1103/PhysRevD.95.115030

Stau Coannihilation, Compressed Spectrum and SUSY Discovery at the LHC

Amin Aboubrahim*, Pran Nath† and Andrew B. Spisak‡

Department of Physics, Northeastern University, Boston, MA 02115-5000, USA

May 16, 2017

Abstract: The lack of observation of supersymmetry thus far implies that the weak supersymmetry scale is larger than what was thought before the LHC era. This observation is strengthened by the Higgs boson mass measurement at ~ 125 GeV which within supersymmetric models implies a large loop correction and a weak supersymmetry scale lying in the several TeV region. In addition if neutralino is the dark matter, its relic density puts further constraints on models often requiring coannihilation to reduce the neutralino relic density to be consistent with experimental observation. The coannihilation in turn implies that the mass gap between the LSP and the NLSP will be small leading to softer final states and making the observation of supersymmetry challenging. In this work we investigate stau coannihilation models within supergravity grand unified models and the potential of discovery of such models at the LHC in the post Higgs boson discovery era. We utilize a variety of signal regions to optimize the discovery of supersymmetry in the stau coannihilation region. In the analysis presented we impose the relic density constraint as well as the constraint of the Higgs boson mass. The range of sparticle masses discoverable up to the optimal integrated luminosity of the HL-LHC is investigated. It is found that the mass difference between the stau and the neutralino does not exceed ~ 20 GeV over the entire mass range of the models explored. Thus the discovery of a supersymmetric signal arising from the stau coannihilation region will also provide a measurement of the neutralino mass. The direct detection of neutralino dark matter is analyzed within the class of stau coannihilation models investigated. The analysis is extended to include multi-particle coannihilation where stau along with chargino and the second neutralino enter in the stau coannihilation process.

1 Introduction

Supersymmetry has not been observed thus far, which implies that its scale is higher than expected before the LHC era. This observation is strengthened by the discovery that the Higgs boson [1–3] mass is ~ 125 GeV [4, 5][1]. Analysis within high-scale supergravity grand unified model [7] (for a review see [8]) show that the loop correction to the Higgs boson mass in supersymmetry must itself be sizable, which in turn implies a larger value for weak supersymmetry scale lying in the

*Email:a.abouibrahim@northeastern.edu

†Email:p.nath@northeastern.edu

‡Email:a.spisak@northeastern.edu

[1]For a review of the status of supersymmetry after the Higgs boson mass measurement at ~ 125 GeV see [6]

several TeV region [9–12]. There is another constraint that explains the possible reason for the lack of detection of a supersymmetric signal. In supergravity grand unified models with R party conservation, neutralino is the LSP over most of the parameter space of models [13] and thus a candidate for dark matter. The annihilation of the neutralino in sufficient amounts to have its relic density consistent with the WMAP and then PLANCK experimental results imposes additional constraints. Specifically if the neutralino is Bino like, one needs coannihilation (for early work see [14]) to have consistency with experiment. However, coannihilation implies that the next to lightest supersymmetric particle (the NLSP) must be close to the LSP with a small mass gap to ensure efficient annihilation of the LSP. The existence of the small mass gap in turn implies that the final states in the decay of the NLSP will be soft making them difficult to detect. Coannihilation appears in supergravity models with universal as well as with non-universal boundary conditions at the grand unification scale which lead to a large sparticle landscape [15]. The large landscape includes non-universalities in the gaugino sector [16, 17] and in the matter and Higgs sectors [18]. We note in passing that often naturalness criteria are used to argue what the scale of weak scale supersymmetry should be. Previously it has been argued that the weak scale could be large and natural on the hyperbolic branch of radiative breaking of the electroweak symmetry [19–25]. Additionally, analyses of naturalness including proton stability from baryon and lepton number violating dimension five operators in grand unified theories (for a review of status see [26]) along with electroweak symmetry breaking constraints tend to favor the weak scale of SUSY in the TeV region [27].

Thus coannihilation necessarily implies that the lightest sparticle spectra which are the prime candidates for detection are compressed. Such compressed spectra can appear in stau coannihilation, stop coannihilation, gluino coannihilation among others (for some recent works on stop coannihilation and gluino coannihilation in the post Higgs boson discovery era see [28, 29]. For recent theory papers related to supersymmetry and compressed spectrum see [30–33] and for experimental searches for supersymmetry with a compressed spectrum see [34–36]). In this work we extend that analysis to the stau coannihilation region under the Higgs boson mass constraint and the relic density constraints. Stau–neutralino coannihilation has previously been investigated by a number of works [31, 37–40]. Specifically in [31] an analysis has been carried out for the stau–neutralino coannihilation region at LHC Run II. However, the analysis of [31] was limited to neutralino masses below 100 GeV and further the Higgs boson mass constraint and the relic density constraints were not imposed. In this work we use nonuniversal supergravity models with nonuniversalities in the gaugino sector to investigate the full range of neutralino and stau masses that are discoverable up to the expected integrated luminosity at the LHC in the future. In our analysis we impose the relic density constraints as well as constraint of the Higgs boson mass. Specifically we use the $\tilde{g}$SUGRA model [41] where the mass for the $SU(3)_C$ gaugino is much larger than the masses for the electroweak gauginos. In this case the universal scalar mass can be rather low lying in the low hundreds of GeV and it is the gluino which drives the radiative breaking giving much larger masses to the squarks while the slepton masses remain low. In this case the stop masses can be large enough to give the desired loop corrections for the Higgs boson mass. Further, the large splitting between the squark masses and the slepton masses allows for the possibility of a stau-neutralino coannihilation. We will also investigate in the $\tilde{g}$SUGRA framework a multi-particle coannihilation where more than two particles participate in the coannihilation process. This happens, for example, if the neutralino, the stau, and the chargino, and the next to lightest neutralino are clustered together. In this case one finds more copious set of signatures for discovery. We use signal regions based on those previously published in [40, 42] but optimized for the stau–neutralino coannihilation region. An analysis of dark matter is also given. Some of the signatures of the $\tilde{g}$SUGRA model were analyzed in [41]

and a more detailed signature analysis and potential for discovery of this model was given in [43]. Here we analyze the discovery potential of $\tilde{g}$SUGRA for a set of benchmark parameter points with optimization of signal regions. A comparison of this analysis with some of the previous work is given at the end of section 4.3

The outline of the rest of the paper is as follows: In section 2 we discuss how a stau-neutralino coannihilation can arise in a high scale model while generating the desired correction to the Higgs boson mass and also satisfying the relic density constraints. We also discuss here the possibility of a multiparticle coannihilation involving the neutralino, the stau, the chargino and the second neutralino. In section 3, we discuss the production of supersymmetric particles for the stau and the multiparticle coannihilation models. Here we exhibit the cross sections for the production of the final states $\tilde{\chi}_2^0\tilde{\chi}_1^\pm$, $\tilde{\chi}_1^+\tilde{\chi}_1^-$, $\tilde{\tau}^+\tilde{\tau}^-$, and $\tilde{\tau}\tilde{\nu}_\tau$. The sparticles in the final states decay with a neutralino and leptons in the final states. The signature analysis of these requires a knowledge of the backgrounds arising from the production and decay of the standard model particles. Here we use the backgrounds published by the SNOWMASS group. Section 4 is devoted to the signature analysis of the high scale models and an analysis of the minimum integrated luminosity needed with the LHC operating at 13 TeV for the 5σ discovery. Here a comparison of the different signature regions is also made and combined signal region results are exhibited where models are arranged in terms of ascending order in the minimum integrated luminosity needed for a 5σ discovery. At the end of this section we give an analysis of dark matter cross sections for the models discussed in sections 2-4. It is shown that the spin independent neutralino-proton cross sections lie significantly above the neutralino floor and some of the models lie close to the lower bounds that will be reached by the next generation direct detection experiments. Conclusions are given in section 5.

2 Stau coannihilation in SUGRA models

We have earlier noted that the observation of the Higgs boson mass at $\sim$ 125 GeV requires a large loop correction to its tree value which is below the Z-boson mass. The largest correction arises from the stop masses in the loop and one needs an average stop mass in the several TeV region. In SUGRA models with universal soft parameters at the grand unification scale, this would indicate a large universal scalar mass m_0 if we wish to have the charginos and the neutralinos at the electroweak scale. A large universal scalar mass would also imply that the sleptons also have few TeV size masses. Thus this set up would not lead to stau coannihilation which requires that the lightest neutralino which we assume to be the LSP and the the lighter stau be in proximity with a mass gap so that $(m_{\tilde{\tau}} - m_{\tilde{\chi}^0})/(m_{\tilde{\tau}} + m_{\tilde{\chi}^0}) \leq 1/20$. In high scale models stau coannihilation can occur with charginos and the neutralinos at the electroweak scale if we lower the universal scalar mass so that the sleptons in general have a mass comparable to the masses of the charginos and the neutralinos. This leads us to non-universal SUGRA models of a specific variety, i.e., where we consider non-universalities in the gaugino sector. Specifically, if we consider the mass of the $SU(3)_C$ gaugino (m_3) at the grand unification scale to be much larger than the masses of the $U(1)_Y$ and $SU(2)_L$ gauginos (m_1, m_2), i.e., $m_3 >> m_1, m_2$. In this class of models which are labeled $\tilde{g}$SUGRA [41], m_0 is chosen to be relatively low of size a few hundred GeV, while m_3 is taken to be relatively large of size in the several TeV. The large m_3 mass drives the squark masses to acquire TeV size masses through renormalization group evolution (for a review see [44]), while the slepton masses remain largely unaffected [41]. This set up allows one to realize stau

coannihilation since both the neutralino and the stau lie in the sub TeV region and can lie close to each other.

The parameter space of this model is thus given by $m_0\,, A_0\,, m_1 = m_2 << m_3\,, \tan\beta\,, \mathrm{sign}(\mu)\,$, where A_0 is the universal trilinear scalar coupling at the grand unification scale, $\tan\beta = \langle H_2\rangle/\langle H_1\rangle$, where H_2 gives mass to the up quarks and H_1 gives mass to the down quarks and the leptons, and $\mathrm{sign}(\mu)$ is the sign of the Higgs mixing parameter which enters in the superpotential in the term $\mu H_1 H_2$. For the multiparticle coannihilation parameter space, we relax the requirement that $m_1 = m_2$, allowing m_2 to lie lower than m_1. This brings the mass of the chargino and second neutralino closer to the stau and the LSP so that those particles also contribute to coannihilation. In this case we use the following parameter space for the model: $m_0\,, A_0\,, m_2 < m_1 << m_3\,,\ \tan\beta\,, \mathrm{sign}(\mu)\,$. Using the above input parameters, the sparticle spectrum is generated using `SoftSUSY 3.7.3` [45, 46] while the analysis of the relic density is done using `micrOMEGAs 4.3.1` [47]. SUSY Les Houches Accord formatted data files are processed using `PySLHA` [48].

First we consider parameter regions of the $\tilde{g}$SUGRA model with the Higgs boson mass of 125 ± 2 GeV where stau–LSP coannihilation gives rise to an LSP relic density within the known limit $\Omega h^2 < 0.128$. A sample set of such points is given in Tables 1 and 2, where Table 1 gives the input parameters and Table 2 gives the sparticle masses for those inputs. As demonstrated in Table 2, the parameter points in the stau coannihilation region have a very small stau–neutralino mass gap $\Delta = (m_{\tilde{\tau}_1} - m_{\tilde{\chi}_1^0}) \sim 20$ GeV. Such a small gap raises many challenges for discovery. In cases with such little energy available for decay jets, initial and final state radiation (ISR and FSR) events are often relied upon to produce a more detectible signal at colliders. Next we consider a model of multipartcle coannihilation among the neutralino (LSP), the stau (NLSP), and the chargino and second neutralino, which in this model remain nearly degenerate. The parameter points of Table 3 are chosen so as to satisfy the constraints on the Higgs boson mass, $m_h = 125\pm2$ GeV, and the relic density $\Omega h^2 < 0.128$ and in such a way as to produce the mass hierarchy $m_{\chi_1^0} < m_{\tilde{\tau}} < m_{\chi_1^\pm} \sim m_{\chi_2^0}$. Some of the sparticle masses corresponding to Table 3 are given in Table 4.

In Fig. 1 we exhibit the sparticle mass hierarchies generated by model point (a) of Table 1. Here the mass hierarchy of some of the low lying sparticles is: $\tilde{\chi}_1^0 < \tilde{\tau}_1 < \tilde{\chi}_1^0 \simeq \tilde{\chi}_1^\pm < \tilde{\nu}_\tau < \tilde{\nu}_L < \tilde{\ell}_L < \tilde{\tau}_2$. In Fig. 2 we exhibit the sparticle mass hierarchies generated by model point (iii) of Table 3. Here the mass hierarchy of some of the low lying sparticles is similar to that for model point (a) of Table 1 except that $\tilde{\tau}_1$, $\tilde{\chi}_2^0$ and $\tilde{\chi}_1^\pm$ are very close in mass. As discussed in [15] the sparticle mass hierarchies including the mass gaps contain significant information regarding the nature of soft breaking at the grand unification scale and Figs. 1 and 2 are an illustration of this phenomenon. Thus observation of low lying sparticles and measurement of their masses will allow us to narrow down in a significant way the nature of the unified model from which the sparticle spectrum originates.

3 Analysis for coannihilation models at LHC at $\sqrt{s} = 13$ TeV

After a scan of the non-universal Supergravity (nuSUGRA) parameter space was performed to select benchmark points for each of the two coannihilation models satisfying the Higgs boson mass constraint, the relic density, and the desired neutralino, stau, and chargino mass hierarchies discussed in the previous section (Tables 1 and 3), those points are then used for a Monte Carlo analysis of LHC signal regions. This analysis was performed with the `MADGRAPH 2.4.2` [49] software system. First, the Feynman diagrams were calculated for all possible decays of the form $pp \rightarrow$ SUSY SUSY, where "SUSY" can be any MSSM particle. The analysis is configured to include both

ISR and FSR jets. With the sparticle spectra of the benchmark points calculated by `SoftSUSY`, as well as the decay widths and branching ratios calculated by `SDECAY` and `HDECAY` operating within `SUSY-HIT` [50], `MADEVENT` was used to simulate 50,000 MSSM decay events for each benchmark point. Hadronization of resultant particles is handled by `PYTHIA 6.4.28` [51], and ATLAS detector simulation and event reconstruction is performed by `DELPHES 3.3.3` [52]. A large set of search analyses were performed on the generated events for each benchmark point. The analyses used `ROOT 5.34.21` [53] to implement the constraints of the search region for the signal regions involving hadronic τ final states and other leptonic final states (see Section 4).

To allow comparison to the background, all of the signal region analyses were applied to pre generated backgrounds published by the SNOWMASS group [54]. For each benchmark point, a calculated implied integrated luminosity allowed direct comparison to the backgrounds. Each individual background process from the SNOWMASS background set was scaled by its own implied integrated luminosity and combined to determine a total background count for each signal region. The various background samples are grouped according to the generated final state, with a collective notation given by

$$\begin{aligned} J &= \{u, \bar{u}, d, \bar{d}, s, \bar{s}, c, \bar{c}, b, \bar{b}\}\,, \\ L &= \{e^+, e^-, \mu^+, \mu^-, \tau^+, \tau^-, \nu_e, \nu_\mu, \nu_\tau\}\,, \\ B &= \{W^+, W^-, Z, \gamma, h^0\}\,, \\ T &= \{t, \bar{t}\}\,, \\ H &= \{h^0\}\,. \end{aligned} \tag{1}$$

In general, events with gauge bosons and the SM Higgs boson in the final state are grouped into a single "boson" (B) category. Thus, for example, the data set "Bjj-vbf" represents production via vector boson fusion of a gauge boson or a Higgs boson with at least two additional light-quark jets. The standard model background is displayed for two kinematic variables M_{eff}(incl.) and E_T^{miss} in Fig. 3.

3.1 LHC production and signal definitions

The signal regions considered here comprise two major categories, based upon the sparticle whose decay signatures they are meant to capture. The first category of signal regions includes signatures based on hadronically decaying taus, which are an expected result of stau decay. The second category involves signatures of multiple light leptons, which are meant to search for the decays of charginos and heavy neutralinos. Because both of the coannihilation regions under investigation have light staus and electroweak gauginos (i.e., charginos and neutralinos heavier than the lightest neutralino), it is expected that both signal region categories are viable for the stau coannihilation models considered here. The first signal region studied in this work involves at most 1 hadronically decaying tau in the final state. The selection criteria for one τ_h are based on an optimization of those defined in [40]. The second set of signal regions looks for at most 2 hadronically decaying taus in the final state. The selection criteria used are a modification of those in [40], where the first (SC1) involves cuts on the transverse momenta of τ_h and the second (SC2) involves cuts on the effective mass, m_{eff}, defined as the sum of the missing transverse energy E_T^{miss} and the transverse momenta of the two leading hadronic taus. These signal regions are discussed in greater detail in Section 4.1. Next we analyze electron and muon signal regions based on the work of [42]. One set of signal regions requires two leptons in the final state, comprising either a same flavor opposite sign pair, or a different flavor opposite sign pair, with increasing cuts on kinematic variables. The

second set requires three leptons in the final state, two of which form a same flavor opposite sign pair. These are discussed further in section 4.2. Using the techniques and signal regions described above, we analyze each of the benchmark points in Tables 1 and 3 to identify a signal region with minimum required integrated luminosity for 5σ S/$\sqrt{\text{B}}$ discovery of that point at the LHC.

4 Signature analysis and results

In Tables 5 and 6 we give an analysis of the sparticle production cross sections for the models under study. The cross section for all models is dominated by the production of the neutralino $\tilde{\chi}_2^0$ and chargino $\tilde{\chi}_1^\pm$. In nearly every model point the only decay mode of $\tilde{\chi}_2^0$ is via the channel $\tilde{\chi}_2^0 \to \tilde{\tau}\tau$, while the primary decay of the chargino is via the channel $\tilde{\chi}_1^\pm \to \tilde{\tau}\nu_\tau$ (see Tables 7 and 8). The stau always decays through one channel, $\tilde{\tau} \to \tilde{\chi}_1^0\tau$ (see Tables 9 and 10), where the available phase space for the emitted tau is small, resulting in a soft tau production making it difficult to observe with low integrated luminosity.

4.1 τ-based signals

We start by discussing the 1τ signature search by applying the selection criteria given in [40]. It turns out that the calculated luminosity necessary for a 5σ discovery lies beyond the maximum integrated luminosity achievable at the LHC. The main problem is the cut on the missing transverse energy. In [40], a cut on E_T^{miss} was made so that $E_T^{\text{miss}} > 230$ GeV. However, for the class of models we consider this cut is not optimal as illustrated in the left panel of Fig. 4. Here one finds that we begin to lose the signal for $E_T^{\text{miss}} > 200$ GeV leading to a small signal to background ratio in this case. Further, the cut on $p_T(\tau_h)$ of [40], i.e., $15 < p_T(\tau_h) < 35$ GeV applied on the hadronic tau transverse momentum is not optimal for the models considered here. The right panel of Fig. 4 shows that signal is above the background in the range $20 - 90$ GeV. Thus increasing the range of cut on $p_T(\tau_h)$ will produce better results. The optimized cuts for the 1τ signature are displayed in Table 11 including three variations: 1τ-A, 1τ-B and 1τ-C. They correspond to variations of the cut on $p_T(\tau_h)$. Table 12 gives the minimum integrated luminosity needed for a 5σ discovery using these cuts on each of the benchmark points of Table 3 which correspond to the multipartcle coannihilation region. The best results are obtained for the cuts of 1τ-A where the luminosity ranges from 1510 to 2650 fb^{-1}, which is less than the optimal integrated luminosity achievable at the LHC, i.e., ~ 3000 fb^{-1}. Results obtained from 1τ-C show, for the most part, luminosities greater than 3000 fb^{-1} since the range of the cut on $p_T(\tau_h)$ extends to 150 GeV, which is above the value at which the signal generally begins dropping below background.

Another τ signature of interest is that of two hadronically decaying taus in the final state. Here we adopt the signal regions of Table 11 to the 2τ case by considering two selection criteria SC1 and SC2 as shown in Table 13. The first selection criterion SC1 is a duplication of the cuts from Table 11, modified to require a second τ, while in the selection criterion SC2 we introduce the variable m_{eff}, defined as the scalar sum of the missing transverse energy and the transverse momenta of the two leading hadronic taus, $m_{\text{eff}} = E_T^{\text{miss}} + p_T^{\tau_{1h}} + p_T^{\tau_{2h}}$. For completeness, we apply those cuts also to the 1τ signal regions and find that this improves our results from Table 12. Thus, the new set of τ based signal regions after inclusion of additional selection criteria SC1 and SC2 are presented in Table 13. Here we veto on electrons, muons, and b-jets. In this set, we have removed the cut on the pseudorapidity of the leading jet which was among the cuts for the 1τ signature in Table 11.

Also, an upper bound has been placed on the $E_T^{\rm miss}$ cut to suppress values where the signal drops below the background. In Fig. 5 we exhibit the distributions in $p_T(j_1)$, the transverse momentum of the leading jet, and the effective mass $m_{\rm eff}$ for the model point (xi). The signal appears to be above the background for lower $p_T(j_1)$ and $m_{\rm Eff}$ values at which the cuts were applied (Table 13).

In Table 14 we give the required minimum integrated luminosities for discovery for points (a)-(k) corresponding to the stau coannihilation model. The 1τ signature performs better than the 2τ for both SRs, SC1 and SC2, thus the reason this channel was omitted from table 14. In 1τSC1 and 1τSC2 all points perform well except h and j. This is because both have the lowest production cross-section (see Table 5) and thus require higher integrated luminosities for discovery. Point (k) has the lowest integrated luminosity of 220 fb^{-1} in 1τSC1-C and point (d) has the highest at 2960 fb^{-1} also in 1τSC1-A. Similarly, we computed the integrated luminosities for benchmark points (i)-(xi) corresponding to the multiparticle coannihilation model. Focusing on the 1τ signature, we notice an improvement compared to what was presented in Table 12. Here all luminosities appear to be well below 3000 fb^{-1} in both SC1 and SC2 and are, thus, within reach of the HL-LHC. Despite having a poorer performance, the 2τ SR and in particular 2τSC2-A gives the lowest luminosity of 73 fb^{-1} for point (xi). It is worth noting that 70% of the points (i)-(xi) have 1τSC1-C as the leading SR while 75% of the points (a)-(k) that are listed have 1τSC1-C as the leading SR. It can be seen that introducing the kinematic variable $m_{\rm eff}$ has improved our results for some regions while it didn't have much effect on others. For example, in the 2τSC2-A, B and C, where this variable is considered, an integrated luminosity less than 100 fb^{-1} is obtained for point (xi) which can be reached by the end of the current LHC run. In addition, for equivalent kinematic cuts, signal regions demanding a single hadronically decaying tau performed better than those demanding two taus for both the multiparticle coannihilation and stau coannihilation regions. It must be noted that the slight differences between the 1τ and 2τ cuts in SC2 is needed to give plausible results for the 2τ channel. Forcing exactly the same cuts produces overall unsatisfactory results for the 2τ channel. Analysis of the discovery potential for supersymmetry for the parameter space of Table 3, using the selection criteria of Table 13, where the minimum integrated luminosity needed for 5σ discovery is displayed in Table 15.

The last SR we will investigate for the 2τ based signal is SR-2τSC3 given in Table 16. The reason for doing so is to try and accommodate most of the variables used by ATLAS in their searches. One of those variables is the quantity $m_{{\rm T}\tau 1} + m_{{\rm T}\tau 2}$ defined as the sum of the transverse masses of the leading and sub-leading taus, where $m_{{\rm T}\tau}$ is calculated from the transverse momentum of the tau and $\mathbf{p}_{\rm T}^{\rm miss}$, so that

$$m_{{\rm T}\tau}(\mathbf{p}_{{\rm T}\tau}, \mathbf{p}_{\rm T}^{\rm miss}) = \sqrt{2(p_{{\rm T}\tau}\, E_{\rm T}^{\rm miss} - \mathbf{p}_{{\rm T}\tau} \cdot \mathbf{p}_{\rm T}^{\rm miss})}, \tag{2}$$

and $\Delta R(\tau_h, \tau_h)$ is the separation between the first two leading taus. Also here we keep our veto on the b-jets, electrons and muons. Table 17 shows the integrated luminosities obtained for three variations of the transverse mass sum pertaining to the multi-particle coannihilation model points (i)-(xi). Signal region 2τSC3-A gives integrated luminosities as low as 670 fb^{-1} (for point xi). However, more than half of the listed points in table 17 have 2τSC3-B as their leading SR. It is clear that for the most part, SC1 and SC2 give better results.
In Figs. 5 to 7 we exhibit the distributions in different kinematical variables for the multiparticle coannihilation model (xi) at 73 fb^{-1} for signal region 2τSC2-A and at 670 fb^{-1} for signal region 2τSC3-A in Fig. 8, where we plot the number of SUSY signal events (red) against the square root of the SM background (blue). The left panel of Fig. 5 shows the distribution in the transverse momentum of the leading jet, $p_T(j_1)$ and the right panel shows the distribution in the effective mass

$m_{\rm eff}$. A similar analysis is done in Fig. 6 for the transverse momentum of the leading hadronic tau, $p_T(\tau_{1h})$ (left panel), and sub-leading $p_T(\tau_{2h})$ (right panel). In Fig. 7 the same analysis is done but for the spatial separation between the subleading hadronic jet and the leading jet, $\Delta R(\tau_{2h}, j_1)$ in the left panel and the missing transverse energy $E_T^{\rm miss}$ in the right panel. The histogram for the sum of the transverse masses of the first two leading hadronic tau jets is shown in the left panel of Fig. 8 and the histogram for the spatial separation between the two leading hadronic taus $\Delta R(\tau_h, \tau_h)$, which is effective in discriminating against back-to-back events such as multi-jet production or Z decays, is exhibited in the left panel. The distributions for two kinematical variables are also plotted for point (iii) in the 2τ channel exhibited in Fig. 9 and showing an excess of the signal over background events.

4.2 e and μ-based signals

In addition to the direct production of τ leptons due to the decay of stau particles, it is expected that decays of charginos and heavy neutralinos will result in detectible light leptons (electrons and muons) upon which further signal regions can be based. To evaluate the effectiveness of these types of searches in regions of stau coannihilation and multiparticle coannihilation, benchmark models of Tables 1 and 3 are evaluated against electroweak gaugino signals designed to search for decays of $\widetilde{\chi}_1^+\widetilde{\chi}_1^-$ and $\widetilde{\chi}_1^\pm\widetilde{\chi}_2^0$ [42]. These signal regions are classified according to the number of signal leptons. In the two lepton case, six signal regions are defined in two broad categories (see Table 18): signal regions labeled as 2l-SF require that the signal leptons form a same flavor, opposite sign (SFOS) pair, while signal regions labeled as 2l-DF require a different flavor, opposite sign (DFOS) pair. The sub-categories A, B, and C in Table 18 indicate different cuts on the kinematic variable $m_{\rm T2}$ [55–57], which is defined as

$$m_{\rm T2} = \min\left[\max\left(m_{\rm T}(\mathbf{p}_{\rm T}(\ell_1), \mathbf{q}_{\rm T}), m_{\rm T}(\mathbf{p}_{\rm T}(\ell_2),\, \mathbf{p}_{\rm T}^{\rm miss} - \mathbf{q}_{\rm T})\right)\right] \tag{3}$$

where $\mathbf{q}_{\rm T}$ is an arbitrary vector chosen to find the appropriate minimum and $m_{\rm T}$ is the transverse mass given by

$$m_{\rm T}(\mathbf{p}_{\rm T1}, \mathbf{p}_{\rm T2}) = \sqrt{2(p_{\rm T1}\, p_{\rm T2} - \mathbf{p}_{\rm T1}\cdot\mathbf{p}_{\rm T2})}. \tag{4}$$

In addition to cutting on $m_{\rm T2}$ and the missing transverse energy $E_T^{\rm miss}$, the three lepton signal regions contain three jet vetoes, requiring that events contain no jets other than very soft jets in three jet categories: b-tagged jets (b-jet veto), jets which are not b-tagged and which have $|\eta| \leq 2.4$ (light jet veto), and jets which are not b-tagged and which have $2.4 \leq |\eta| \leq 4.5$ (forward jet veto). Finally, for the 2l-SF signal regions, there is a Z veto which requires that the invariant mass of the SFOS lepton pair not lie within 10 GeV of the Z mass. iThe p_T of the leading and sub-leading leptons are required to exceed 25 GeV and 20 GeV, respectively. For the three lepton case, two of the leptons are required to comprise a SFOS pair, with the third lepton allowed to have the same or different flavor. For the case where all three leptons are the same flavor, the SFOS pair is chosen to be that whose invariant mass is closest to the Z mass. The three lepton case admits two signal regions A and B, with B representing tighter cuts on relevant kinematic variables (see Table 19). Here, in addition to a veto on b-tagged jets, cuts are applied to the missing transverse energy, the transverse momentum of the third lepton, the transverse mass as defined above, and the invariant mass of the SFOS pair.

With these signal regions, it is possible to assess the discovery potential of stau coannihilation region parameter points based on the signal from electroweak gaugino decays. Tables 20, 21,

and 22 below describe the results in terms of the integrated luminosity in fb^{-1} required for a 5σ discovery. Results for the three lepton signal regions described in Table 19 are not displayed because it is found that in all cases, the required luminosity for discovery was much larger than for the two lepton cases, indeed larger than the 3000 fb^{-1}. This is due to the fact that the decay events from these coannihilation regions almost never produce three final state leptons. We find that for the leptonic signal regions, as mentioned earlier it is only the two lepton signals that give promising results. Of these, the signal regions which require a SFOS pair perform much better than those requiring a DFOS pair. Thus, this specific signal region topology is found to be the best leptonic signal for the stau and multiparticle coannihilation regions. The remaining variation is upon kinematic cuts, in this case the cut on the variable $m_{\rm T2}$. As expected for a kinematic cut, the softer cut of 2l-SF-A is optimal for lower mass benchmark points, while the harder cut 2l-SF-C is optimal for higher mass points. The intermediate signal region 2l-SF-B was not optimal for any case studied. Figs. 10 and 11 display the $m_{\rm T2}$ and $E_T^{\rm miss}$ kinematic variables for signal and combined background after cuts. Fig. 10 gives counts in $m_{\rm T2}$ after the 2l-SF-A signal region cuts for models (k) and (c), models for which that signal region is optimal, displayed at the integrated luminosity calculated as necessary for discovery. Fig. 11 gives counts in the same signal region and for the same models, but this time in the $E_T^{\rm miss}$ kinematic variable.

4.3 Combined Signal Region Results

As an overall view of the signal regions considered and their success in discriminating between signal and background, we list in Tables 23 and 24 the leading and sub-leading signal regions and the corresponding model points for the stau and multiparticle coannihilation regions, respectively. Model points are listed in an ascending order of luminosity. The analysis of Tables 23 and 24 shows that probing the supersymmetric signals originating from the stau coannihilation and multiparticle coannihilation regions would be challenging. By the end of this year the CMS experiment is expected to collect about 45-50 fb^{-1} of data [58] and one expects similar amount of data from the ATLAS experiment [59]. One expects that by the time the LHC RUN II is over one may have a large enough data set to probe part of the stau and multiparticle coannihilation regions specifically model k of Table 23 which can be probed with 97 fb^{-1} of integrated luminosity and model xi of Table 24 which can be probed with 73 fb^{-1} of integrated luminosity. Of course after the high luminosity LHC upgrade, HL-LHC is expected to collect up to 3 ab^{-1} of data at a center-of-mass energy of 14 TeV. Thus with this data the full set of models listed in Tables 23 and 24 can be tested. We note here that the dark matter constraints would become even more severe if the neutralino contributed only a fraction of the dark matter density in the universe as is the case in multi-component dark matter models (see e.g., [60]). One recent entry is the ultralight boson [61–63] needed to explain cosmology at small scales which could contribute part of the relic density of dark matter. In this case the mass gaps between the neutralino and the stau would have to be even narrower to reduce the dark matter relic density to a fraction of the observed one. One item not addressed in this analysis and which needs further study, is the effect of pile up (for a review of these effects see [64]). Such an analysis is outside the scope of the current work but would be a topic of further study.

Next we compare our analysis with that of the recent analysis of the ATLAS Collaboration [42]. To begin with we note that the analysis of [42] is based on simplified models and the details of these models in terms of the relative ratios of the sleptons and the electroweak gauginos are very

different from the ones that arise in our analysis which is based on a high scale model. This also applies to the branching ratios of the decays of the electroweak gauginos used by [42] which are again very different from our case. Thus some of the regions excluded in the analysis of [42] are not excluded for the high scale models we consider.

In further comparison of our analysis with that of [42], we note that in all of our analysis we use the full SUSY production cross sections. Thus the total sfermion production cross section includes the electroweak gaugino, stau as well as slepton ($\tilde{e}, \tilde{\mu}$) production cross sections. We first compare our results of table 2 based on the parameter set of Table 1 with the exclusion plots of Fig 7 of [42]. The analysis of Fig. 7 of ref [42] uses a common first two generation slepton mass of $(m_{\tilde{\chi}_1^0} + m_{\chi_1^+})/2$. Further, they assume a 100% branching ratio of the decay of the chargino into sleptons. Both these assumptions are not valid for the parameter points of Table 1 and the spectrum it generates as given by Table 3. In any case the chargino and the neutralino mass spectrum of Table 2 lies outside the blue area adjoining the y-axis in Fig. 7a and is thus not excluded. Further, there are no significant 3 lepton signals for the cases we consider and thus the analysis of Fig. 7b of ref [42] does not apply. So in this case both the analysis of [42] and our analysis are in agreement regarding the parameter points of Table 1 and the spectrum of Table 3 which are not excluded by the current data.

Next we consider the parameter set of Table 3 and the corresponding sparticle spectrum given by Table 4. Essentially all the observations made in the context of Table 1 and Table 2 are also valid in this case. Specifically we can see from Table 4 that the masses of $\tilde{e}_L, \tilde{e}_R, \tilde{\mu}_L, \tilde{\mu}_R$ are significantly higher than the chargino mass and thus the chargino can only decay into the light stau; it has no branching ratio into sleptons. In contrast the analysis of [42] assumes 100% branching ratio into $\tilde{e}, \tilde{\mu}$ sleptons and therefore its exclusion plots do not apply to our analysis. Specifically most of the parameter points of Table 3 and of Table 4 lie inside the blue excluded region of Fig. 7a of [42] pointing to the danger of using simplified modes which are based on ad hoc assumptions and do not arise from any underlying theory to exclude valid regions of the parameter space of supergravity models.

We made further checks on our analysis. Most of the multiparticle coannihilation points (table 3) have a suppressed production cross-section for sleptons. For example, for point (i) the total SUSY production cross-section is 3.99 pb which as we mentioned is dominated by the production of $\tilde{\chi}^{\pm}$ and $\tilde{\chi}_2^0$. Of the 3.99 pb, the sfermion production cross-section is 0.161 pb, of which the production of staus comprises 0.1 pb and the production of sleptons comprises 0.061 pb. There are some exceptions: for example for point (iii) of table 4, the total cross-section is 6.17 pb with the sfermion production cross-section making around 0.14 pb of the total production cross-section. Of the 0.14 pb, 0.073 pb goes for the production of staus and 0.067 for the sleptons. Here the production of sleptons is comparable to the staus, explaining the strong lepton signal in the final state for this point. The 6th column of table 24 shows the sub-leading leptonic signal region which, for some points, gives integrated luminosities comparable to that of the leading and sub-leading hadronic signal regions. Note that, the production cross-section of sleptons is less that staus since they are heavier.

As a further check on why the analysis of [42] is invalid in our case, we consider point (xi) which has the lightest LSP with mass of 89.9 GeV and a chargino of mass 131.5 GeV. Following [42] we take the slepton masses to be as assumed by ATLAS. To get the relic density we require the

mass gap between the chargino and neutralino to be around 20 GeV and their average to be the slepton mass (246 GeV in this case), then a simple calculation leads to chargino and neutralino masses of ~ 256 GeV and ~ 236 GeV. Referring to Fig. 7 of [42] we see that this parameter point is not excluded. A similar analysis can be carried out for the parameter set of table 1 and the corresponding sparticle spectrum of table 2. Taking the lightest point of the spectrum, namely, point (k) and following the assumption of [42] regarding the slepton, chargino and neutralino mass and requiring a mass gap of around 20 GeV, we find a chargino and neutralino masses of ~ 254 and 234 GeV, respectively, which according to Fig. 7 of [42] are not excluded. For this set of stau coannihilation points, as discussed above, the full SUSY cross-section has been calculated and used in our analysis. Also for point (k), we found that the production cross-section of electroweak gauginos is the dominant process making up 2.4 pb of the total cross-section 2.65 pb. The direct stau production cross-section amounts to 0.144 pb while that of the slepton is 0.105 pb. It is clear that the slepton cross-section is less than that of the stau but nonetheless not insignificant. An example of a slepton production cross-section which is comparable to that of the stau can be seen for point (j). For this point, the production cross-section of staus is 0.01 pb while that of sleptons is 0.011 pb which clearly shows that a signal of leptons in the final state would compete with that of the tau.

We note that the simulation of the SUSY signals was performed at 14 TeV to match the SNOWMASS SM backgrounds. If one considers 13 TeV, then, as an example, for point (x) of Table 3 one gets a production cross-section of 1.44 pb instead of 1.63 pb. As for point (xi), one gets 9.19 pb instead of 10.19 pb. Thus there is around a 10% difference which one supposes would not have a major impact on the 5σ discovery limit on integrated luminosity. It is not possible, however, to predict the exact integrated luminosity for a 5σ discovery at 13 TeV since the SNOWMASS SM backgrounds are not available at 13 TeV.

Next we give a comparison of our work with that of a previous analysis [43] which carried out simulations of the $\tilde{g}$SUGRA model. A direct comparison of our results with that of [43] is difficult because of the following reasons: (i) The analysis of [43] gives only scatter plots in the space of sparticle masses and of the input parameters whereas we work with a list of benchmarks. (ii) The analysis of [43] is done at 300 fb^{-1} in Fig. 9 of that work at 14 TeV while our analysis at 14 TeV looks for minimum integrated luminosity for 5σ discovery limit. (iii) We have carried out an optimization of the signal regions for SUSY discovery focused on the model points considered but it is not clear what has been done in this regard in the analysis of [43]. However, with these caveats a comparison of this work with that of [43], where possible, shows consistency of the two analyses.

4.4 Stau coannihilation and direct detection of dark matter

The analysis presented in Tables 23 and 24 give us a set of models which are consistent with the Higgs boson mass constraint and the constraints on the relic density consistent with the WMAP [65] and the PLANCK experiment [66] and arise from the stau or stau-chargino-second neutralino coannihilation regions. It is of interest to investigate if these models are discoverable in direct detection experiment. For these models the neutralino is mostly a Bino. Thus the neutralino is a linear combination of four states $\tilde{\chi}^0 = \alpha\lambda^0 + \beta\lambda^3 + \gamma\tilde{H}_1 + \delta\tilde{H}_2$ where λ^0, λ^3 are the Bino, Wino and $\tilde{H}_1, \tilde{H}_2$ are the Higgsinos. For the models of Table 1, $|\beta| \leq 0.003, |\gamma| \leq 0.015, |\delta| \leq 0.002$. while for models of Table 3, $|\beta| \leq 0.039, |\gamma| \leq 0.014, |\delta| \leq 0.002$. One finds that the Wino and the Higgsino content of the models of Tables 1 and 3 are small, and the neutralino is essentially

a Bino. This makes the neutralino-proton cross sections relatively small. In Table 25 we present the spin independent and spin-dependent neutralino-proton cross sections for these models. The analysis of Table 25 shows that the spin-independent neutralino-proton cross section though small and $O(10^{48}\text{cm}^{-2})$ still lies significantly above the neutrino floor [67] which is the minimum threshold for detectability (see Fig. 12). Some of the models also lie close to the lower bounds that the future dark matter experiments LUX-ZEPLIN [68, 69] would be able to reach.

5 Conclusions

Supersymmetry is desirable for a number of theoretical as well as phenomenological reasons. Supergravity unification provides a framework for high scale models with a small number of parameters in terms of which the properties of low energy effective theory can be computed. The observation of the Higgs boson mass at ~ 125 GeV implies that the loop correction to the tree level Higgs boson mass is large which in turn implies that the scale of weak scale supersymmetry lies in the TeV region. This makes the search for supersymmetry more challenging than initially thought. For high scale models, there is another aspect which makes the observation of supersymmetry challenging. This concerns dark matter. For high scale models one finds that often the parameter space that gives the desired Higgs boson mass gives a neutralino which is mostly a Bino. For a Bino type neutralino, one needs coannihilation to achieve the appropriate relic density consistent with the WMAP and PLANCK experiment. This means that there must be one or more sparticles close by to coannihilate with the neutralino. The relatively small mass gap between the neutralino and the coannihilating particles implies that the final states in the decay of the coannihilating particles must be soft and thus hard to detect. In this work we have addressed this question in the context of stau coannihilation . We have analyzed two types of models: one type which involves only a two particle coannihilation between the neutralino and the stau, and the second type where the neutralino coannihilates with a stau, a chargino and a second neutralino. We have carried out an extensive signature analysis including a variety of signatures including one tau and two tau final states as well as e and μ final states. Our analysis shows that a variety of signatures exist where the neutralino-stau coannihilation and the neutralino-stau-chargino-second neutralino coannihilation can be discovered with the total integrated luminosity expected at the LHC in future. We also analyzed the spin-independent neutralino proton cross section. It is found that the cross section lies significantly above the neutrino floor and some parts of the parameter space may be accessible in future dark matter experiments such as LUX and ZEPLIN and XENON1T.

Acknowledgments: Computational time allocation at the high-performance Cluster353 at the Advanced Scientific Computing Initiative (ASCI) and the Discovery Cluster at Northeastern University is acknowledged. Also acknowledged are conversations with Bhaskar Dutta, Toyoko Orimoto and Baris Altunkaynak. This research was supported in part by the NSF Grants PHY-1314774 and PHY-1620575.

6 Tables

Model	m_0	A_0	$m_1 = m_2$	m_3	$\tan\beta$
a.	286	-523	314	3015	10
b.	297	-553	343	3246	10
c.	267	-378	367	2911	10
d.	295	-491	381	2821	13
e.	325	-416	412	3156	14
f.	317	-497	437	3065	14
g.	364	-587	445	3728	14
h.	412	-904	503	4688	13
j.	337	833	593	3626	15
k.	295	-551	302	3165	10

Table 1: Input parameters for representative stau coannihilation benchmark points. All masses are in GeV.

Model	h^0	$\tilde{\tau}$	$\tilde{e}_L$	$\tilde{e}_R$	$\tilde{\mu}_L$	$\tilde{\mu}_R$	$\tilde{\chi}_1^0$	$\tilde{\chi}_1^\pm$	$\tilde{t}$	$\tilde{g}$	Ω
a.	123.2	134.4	251.5	318.3	251.5	318.3	112.4	208.4	4522	6168	0.125
b.	123.4	144.3	262.4	333.0	262.4	333.0	123.9	229.7	4842	6608	0.121
c.	123.1	155.1	269.3	309.0	269.3	309.0	136.5	256.0	4376	5961	0.119
d.	123.1	163.9	309.9	335.6	309.9	335.6	143.7	270.7	4244	5787	0.115
e.	123.2	176.7	335.3	367.6	335.3	367.6	155.5	292.2	4720	6428	0.133
f.	123.3	188.9	346.7	364.7	346.7	364.7	167.3	315.5	4584	6251	0.126
g.	123.4	190.3	356.4	409.3	356.4	409.3	167.0	312.0	5506	7517	0.125
h.	123.9	212.0	373.7	464.3	373.7	464.3	187.4	347.6	6775	9287	0.126
j.	123.7	254.0	423.5	409.2	423.5	409.2	232.9	439.5	5422	7308	0.116
k.	123.2	121.9	243.7	325.3	243.7	325.3	106.2	195.3	4732	6456	0.072

Table 2: The Higgs boson (h^0) mass, some relevant sparticle masses, and the relic density for the stau coannihilation benchmark points of Table 1. All masses are in GeV.

Model	m_0	A_0	m_1	m_2	m_3	$\tan\beta$
i.	345	68	394	287	3690	10
ii.	385	152	403	290	3972	12
iii.	318	248	357	249	2973	12
iv.	386	-47	401	284	3809	13
v.	367	78	409	290	3550	13
vi.	423	-19	431	314	4396	13
vii.	353	202	427	298	3351	13
viii.	390	-161	440	308	3864	13
ix.	321	246	423	296	3328	10
x.	432	264	494	350	4234	15
xi.	304	-745	260	221	2793	11

Table 3: Input parameters for representative stau–chargino coannihilation benchmark points. All masses are in GeV.

Model	h^0	$\tilde{\tau}$	$\tilde{e}_L$	$\tilde{e}_R$	$\tilde{\mu}_L$	$\tilde{\mu}_R$	$\tilde{\chi}_1^0$	$\tilde{\chi}_1^\pm$	$\tilde{t}$	$\tilde{g}$	Ω
i.	123.8	161.4	259.9	382.1	259.9	382.1	142.3	171.7	5511	7468	0.124
ii.	123.8	166.5	290.6	420.1	290.6	420.1	144.6	169.7	5912	8007	0.127
iii.	123.2	150.2	265.1	350.3	150.2	265.1	130.4	151.4	4521	6098	0.114
iv.	123.6	166.9	302.3	420.8	302.3	420.8	145.0	167.9	5677	7698	0.115
v.	123.6	171.4	300.8	403.7	300.8	403.7	150.2	177.8	5320	7201	0.120
vi.	123.8	176.5	316.8	459.9	316.8	459.9	154.7	183.9	6488	8808	0.107
vii.	123.5	179.6	302.2	392.9	302.2	392.9	159.3	188.2	5045	6818	0.117
viii.	123.8	182.8	314.3	430.1	314.3	430.1	162.2	188.5	5742	7797	0.103
ix.	123.6	175.1	265.1	363.7	265.1	363.7	157.3	185.9	5011	6773	0.121
x.	123.5	206.5	358.0	475.6	358.0	475.6	184.0	219.0	6272	8492	0.101
xi.	123.1	121.6	246.4	327.4	246.4	327.4	89.9	131.5	4212	5756	0.125

Table 4: The Higgs boson mass, some relevant sparticle masses, and the relic density for the stau–chargino coannihlation benchmark points of Table 3. All masses are in GeV.

Model	full SUSY	$\tilde{\chi}_2^0\tilde{\chi}_1^\pm$	$\tilde{\chi}_1^+\tilde{\chi}_1^-$	$\tilde{\tau}^+\tilde{\tau}^-$	$\tilde{\tau}\tilde{\nu}_\tau$
a.	2.09	2.57	0.62	0.04	0.03
b.	1.48	0.88	0.43	0.03	0.03
c.	1.01	0.58	0.29	0.02	0.02
d.	0.79	0.47	0.23	0.02	0.01
e.	0.59	0.35	0.17	0.01	0.01
f.	0.44	0.26	0.13	0.01	0.007
g.	0.46	0.28	0.13	0.01	0.008
h.	0.31	0.18	0.09	0.007	0.006
j.	0.12	0.07	0.03	0.003	0.002
k.	2.65	1.61	0.79	0.06	0.04

Table 5: SUSY production cross sections in picobarns for stau coannihilation benchmark points of Table 1.

Model	full SUSY	$\tilde{\chi}_2^0\tilde{\chi}_1^\pm$	$\tilde{\chi}_1^+\tilde{\chi}_1^-$	$\tilde{\tau}^+\tilde{\tau}^-$	$\tilde{\tau}\tilde{\nu}_\tau$
i.	3.99	2.57	1.26	0.02	0.03
ii.	4.12	2.68	1.32	0.02	0.02
iii.	6.17	4.02	1.98	0.03	0.03
iv.	4.25	2.78	1.37	0.02	0.02
v.	3.48	2.27	1.11	0.02	0.02
vi.	3.08	2.01	0.98	0.02	0.02
vii.	2.84	1.84	0.90	0.02	0.01
viii.	2.81	1.83	0.90	0.01	0.01
ix.	3.01	1.93	0.94	0.02	0.02
x.	1.63	1.06	0.52	0.01	0.01
xi.	10.19	6.65	3.29	0.06	0.04

Table 6: SUSY production cross sections in picobarns for multiparticle coannihilation benchmark points of Table 3.

Model	$\tilde{\chi}_2^0 \to \tilde{\tau}\tau$	$\tilde{\chi}_1^\pm \to \tilde{\tau}\nu_\tau$
a.	1.00	1.00
b.	1.00	1.00
c.	0.99	0.99
d.	1.00	1.00
e.	1.00	1.00
f.	1.00	1.00
g.	1.00	1.00
h.	0.99	0.99
j.	0.75	0.75
k.	1.00	0.99

Table 7: Branching ratios for dominant decays of $\tilde{\chi}_1^\pm$ and $\tilde{\chi}_2^0$ for stau coannihilation benchmark points of Table 1.

Model	$\tilde{\chi}_2^0 \to \tilde{\tau}\tau$	$\tilde{\chi}_2^0 \to \tilde{\chi}_1^0\tau^+\tau^-$	$\tilde{\chi}_1^\pm \to \tilde{\tau}\nu_\tau$
i.	1.00	0.00	1.00
ii.	1.00	0.00	1.00
iii.	0.00	0.99	1.00
iv.	0.00	0.99	1.00
v.	1.00	0.00	1.00
vi.	1.00	0.00	1.00
vii.	1.00	0.00	1.00
viii.	1.00	0.00	1.00
ix.	1.00	0.00	1.00
x.	1.00	0.00	1.00
xi.	1.00	0.00	1.00

Table 8: Branching ratios for dominant decays of $\tilde{\chi}_1^\pm$ and $\tilde{\chi}_2^0$ for multiparticle coannihilation benchmark points of Table 3.

Model	$\tilde{\tau} \to \tilde{\chi}_1^0\tau$	$\tilde{\nu}_\tau \to \tilde{\chi}_1^0\nu_\tau$	$\tilde{\nu}_\tau \to \tilde{\chi}_2^0\nu_\tau$	$\tilde{\nu}_\tau \to \tilde{\chi}_1^\pm\tau$	$\tilde{\nu}_\tau \to \tilde{\tau}W^\pm$
a.	1.00	0.38	0.07	0.13	0.42
b.	1.00	0.42	0.02	0.03	0.53
c.	1.00	0.47	0.00	0.00	0.53
d.	1.00	0.17	0.01	0.03	0.79
e.	1.00	0.12	0.01	0.02	0.85
f.	1.00	0.13	0.002	0.004	0.87
g.	1.00	0.11	0.006	0.13	0.87
h.	1.00	0.12	0.00	0.00	0.88
j.	1.00	0.10	0.00	0.00	0.90
k.	1.00	0.31	0.08	0.15	0.46

Table 9: Branching ratios for dominant decays of $\tilde{\tau}$ and $\tilde{\nu}_\tau$ for stau coannihilation benchmark points of Table 1.

Model	$\tilde{\tau} \to \tilde{\chi}_1^0 \tau$	$\tilde{\nu}_\tau \to \tilde{\chi}_1^0 \nu_\tau$	$\tilde{\nu}_\tau \to \tilde{\chi}_2^0 \nu_\tau$	$\tilde{\nu}_\tau \to \tilde{\chi}_1^\pm \tau$	$\tilde{\nu}_\tau \to \tilde{\tau} W^\pm$
i.	1.00	0.16	0.27	0.56	0.00
ii.	1.00	0.11	0.23	0.46	0.20
iii.	1.00	0.12	0.25	0.51	0.12
iv.	1.00	0.09	0.20	0.41	0.30
v.	1.00	0.10	0.21	0.42	0.28
vi.	1.00	0.09	0.18	0.37	0.36
vii.	1.00	0.11	0.22	0.44	0.23
viii.	1.00	0.09	0.20	0.41	0.29
ix.	1.00	0.18	0.27	0.55	0.00
x.	1.00	0.07	0.15	0.30	0.48
xi.	1.00	0.12	0.23	0.47	0.18

Table 10: Branching ratios for dominant decays of $\tilde{\tau}$ and $\tilde{\nu}_\tau$ for multiparticle coannihilation benchmark points of Table 3.

Requirement	Value		
	1τ-A	1τ-B	1τ-C
E_T^{miss} (GeV) $>$	130	130	130
$p_T(j_1)$ (GeV) $>$	100	100	100
$\lvert\eta(j_1)\rvert <$	2.5	2.5	2.5
$p_T(\tau_h)$ (GeV) $>$	15	15	20
$p_T(\tau_h)$ (GeV) $<$	50	80	150
$\lvert\eta(\tau_h)\rvert <$	2.3	2.3	2.3
$\Delta R(\tau_h, j_1) >$	0.4	0.4	0.4

Table 11: The selection criteria used for the signal regions with one hadronically decaying tau in the final state and a veto on electrons, muons and b-jets. The angles are in rad.

Model	$\mathcal{L}$ for 5σ discovery in 1τ-A	$\mathcal{L}$ for 5σ discovery in 1τ-B	$\mathcal{L}$ for 5σ discovery in 1τ-C
i.	1510	1810	2520
ii.	1550	1800	2630
iii.	1550	1910	2730
iv.	1580	2020	2930
v.	1800	2260	$\cdot\cdot$
vi.	2010	2290	$\cdot\cdot$
vii.	2010	2330	$\cdot\cdot$
viii.	2090	2340	$\cdot\cdot$
ix.	2400	2880	$\cdot\cdot$
x.	2650	$\cdot\cdot$	$\cdot\cdot$
xi.	1610	1420	1720

Table 12: Analysis of the discovery potential for supersymmetry for the parameter space of Table 3, using the selection criteria of Table 11, where the minimum integrated luminosity needed for 5σ discovery is given in fb^{-1}. Here and in the tables following two dots ($\cdot\cdot$) indicate that the minimum integrated luminosity needed for 5σ discovery exceeds 3000 fb^{-1}.

Requirement	SC1					
	1τ-A	1τ-B	1τ-C	2τ-A	2τ-B	2τ-C
$p_T(j_1)$ (GeV) $>$	20	20	20	20	20	20
$p_T(j_1)$ (GeV) $<$	100	100	100	100	100	100
$p_T(\tau_{1h})$ (GeV) $>$	20	20	20	20	20	20
$p_T(\tau_{1h})$ (GeV) $<$	50	70	90	50	70	90
$p_T(\tau_{2h})$ (GeV) $>$	-	-	-	20	20	20
$p_T(\tau_{2h})$ (GeV) $<$	-	-	-	40	50	60
$\lvert\eta(\tau_{1h})\rvert <$	1.2	1.2	1.2	1.2	1.2	1.2
$\lvert\eta(\tau_{2h})\rvert <$	-	-	-	1.0	1.0	1.0
$\Delta R(\tau_{1h}, j_1) >$	0.6	0.6	0.6	0.6	0.6	0.6
$\Delta R(\tau_{1h}, j_1) <$	1.8	1.8	1.8	1.8	1.8	1.8
$\Delta R(\tau_{2h}, j_1) >$	-	-	-	2.3	2.3	2.3
$\Delta R(\tau_{2h}, j_1) <$	-	-	-	3.3	3.3	3.3
$N(\tau_h)$	1	1	1	2	2	2
Requirement	SC2					
	1τ-A	1τ-B	1τ-C	2τ-A	2τ-B	2τ-C
$p_T(j_1)$ (GeV) $>$	20	20	20	-	-	-
$p_T(j_1)$ (GeV) $<$	200	200	200	110	110	110
$\lvert\eta(\tau_{1h})\rvert <$	1.2	1.2	1.2	1.4	1.4	1.4
$\lvert\eta(\tau_{2h})\rvert <$	-	-	-	1.0	1.0	1.0
$\Delta R(\tau_{1h}, j_1) >$	0.6	0.6	0.6	0.8	0.8	0.8
$\Delta R(\tau_{1h}, j_1) <$	1.8	1.8	1.8	1.8	1.8	1.8
$\Delta R(\tau_{2h}, j_1) >$	-	-	-	2.3	2.3	2.3
$\Delta R(\tau_{2h}, j_1) <$	-	-	-	3.3	3.3	3.3
$m_{\text{eff}} >$	120	130	140	110	110	110
$m_{\text{eff}} <$	200	250	300	250	350	450
$N(\tau_h)$	1	1	1	2	2	2

Table 13: The selection criteria (SC) used for the signal regions with the 1τ and 2τ signatures. The SRs SC1 and SC2 have a common cut on the missing transverse energy of 100 GeV $< E_T^{\text{miss}} <$ 200 GeV, with a veto on electrons, muons and b-jets. The dashes mean that the kinematical variable is not applicable to the corresponding SR. The angles are in rad.

	$\mathcal{L}$ for 5σ discovery in SC1			$\mathcal{L}$ for 5σ discovery in SC2		
Model	1τ-A	1τ-B	1τ-C	1τ-A	1τ-B	1τ-C
a.	786	487	303	745	383	313
b.	1310	674	416	1120	621	536
c.	2760	1280	756	2460	1340	1020
d.	2960	1490	967	2840	1470	1050
e.	··	2860	1700	··	2170	1660
f.	··	··	2210	··	··	2340
g.	··	··	2460	··	··	2340
k.	427	279	220	644	349	299

Table 14: Analysis of the discovery potential for supersymmetry for the parameter space of Table 1, using the selection criteria of Table 13, where the minimum integrated luminosity needed for 5σ discovery is given in fb^{-1}. Points (h) and (j) are not listed because the integrated luminosity for discovery exceeds 3000 fb^{-1}. Only 1τ signal regions are displayed, as those are the signal regions which give luminosities for discovery in the reasonable range.

	$\mathcal{L}$ for 5σ discovery in SC1						$\mathcal{L}$ for 5σ discovery in SC2					
Model	1τ-A	1τ-B	1τ-C	2τ-A	2τ-B	2τ-C	1τ-A	1τ-B	1τ-C	2τ-A	2τ-B	2τ-C
i.	1020	704	625	1090	2460	1290	1040	715	694	477	579	582
ii.	501	380	292	-	-	-	536	370	352	-	-	-
iii.	637	512	472	458	1030	542	827	669	648	200	243	244
iv.	677	575	532	-	-	-	941	695	666	··	··	··
v.	654	475	411	1440	1440	1710	1070	894	898	631	765	770
vi.	898	853	650	-	-	-	1170	743	693	1810	2200	2210
vii.	730	605	508	··	··	··	1190	825	870	··	··	··
viii.	1040	746	660	2200	··	2060	1250	889	842	2170	1170	1170
ix.	1190	713	661	··	··	··	1610	1020	1020	842	575	578
x.	1430	1230	1090	··	··	··	1950	1340	1270	2880	··	··
xi.	265	169	144	168	378	199	176	143	119	73	89	90

Table 15: Analysis of the discovery potential for supersymmetry for the parameter space of Table 3, using the selection criteria of Table 13, where the minimum integrated luminosity needed for 5σ discovery is given in fb^{-1}. The dashes mean that zero events have passed the applied cuts.

Requirement	SR-SC3		
	2τ-A	2τ-B	2τ-C
$E_T^{\rm miss}$ (GeV) $>$	100	100	100
$E_T^{\rm miss}$ (GeV) $<$	200	200	200
$p_T(j_1)$ (GeV) $<$	180	180	180
$m_{\rm eff}$ (GeV) $>$	130	130	130
$m_{\rm eff}$ (GeV) $<$	200	200	200
$m_{{\rm T}\tau 1} + m_{{\rm T}\tau 2} >$	100	100	50
$m_{{\rm T}\tau 1} + m_{{\rm T}\tau 2} <$	200	300	500
$\Delta R(\tau_h, \tau_h) >$	2.5	2.5	2.5
$\Delta R(\tau_h, \tau_h) <$	3.5	3.5	3.5

Table 16: The selection criteria used for the signal regions SR-SC3 with 2 hadronically decaying taus in the final state ($N(\tau_h) = 2$) and a veto on electrons, muons and b-jets.

Model	$\mathcal{L}$ for 5σ discovery in 2τ-SC3-A	$\mathcal{L}$ for 5σ discovery in 2τ-SC3-B	$\mathcal{L}$ for 5σ discovery in 2τ-SC3-C
i.	1240	1090	1430
ii.	1820	1560	1720
iii.	1170	1180	1730
v.	1640	1450	2130
vii.	1710	1540	2270
viii.	2870	2510	··
x.	2690	2700	··
xi.	670	674	991

Table 17: Analysis of the discovery potential for supersymmetry for the parameter space of Table 3, using the selection criteria of Table 16, where the minimum integrated luminosity needed for 5σ discovery is given in fb^{-1}. Models (iv), (vi) and (ix) are not listed because the minimum integrated luminosity needed for 5σ discovery exceeded 3000 fb^{-1}.

Requirement	SF			DF		
	$2l$-SF-A	$2l$-SF-B	$2l$-SF-C	$2l$-DF-A	$2l$-DF-B	$2l$-DF-C
$E_T^{\rm miss}$ (GeV) $>$	100	100	100	100	100	100
light jet p_T (GeV) $<$	20	20	20	30	30	30
b-jet p_T (GeV) $<$	20	20	20	20	20	20
forward jet p_T (GeV) $<$	30	30	30	30	30	30
$\lvert m_{\ell\ell} - m_Z \rvert$ (GeV) $>$	10	10	10	-	-	-
m_{T2} (GeV) $>$	90	120	150	90	120	150

Table 18: The selection criteria used for the signal regions related to the 2 lepton signature, based upon the 2 lepton signal regions from [42]. Here and in the Tables following SF stands for same flavor opposite sign lepton pair and DF stands for different flavor opposite sign lepton pair. A dash denotes a cut which is not applicable to the given signal region.

Requirement	Value	
	$3l$-A	$3l$-B
$E_T^{\rm miss}$ (GeV) $>$	120	100
$p_T(\ell_3)$ (GeV) $>$	30	80
m_T (GeV) $<$	110	110
$m_{\rm SFOS}$ (GeV)	$\notin [21.2, 101.2]$	> 101.2
N(b-jet)	0	0

Table 19: The selection criteria used for the signal regions related to the 3 lepton signature, based upon the 2 lepton signal regions from [42].

	$\mathcal{L}$ for 5σ discovery in 2l-SF		
Model	$2l$-SF-A	$2l$-SF-B	$2l$-SF-C
a.	187	266	266
b.	362	420	441
c.	165	188	169
d.	781	953	884
e.	1480	1630	1700
f.	1110	1380	1250
g.	1850	1850	1790
h.	1860	2050	1660
j.	2160	2250	1880
k.	97	185	225

Table 20: Analysis of the discovery potential for supersymmetry for the parameter space of Table 1, using the 2 lepton same flavor (SF) selection criteria of Table 18, where the minimum integrated luminosity needed for 5σ discovery is given in fb^{-1}. The different flavor (DF) signal regions are omitted due to poor performance (i.e. requiring over 3000 fb^{-1} of integrated luminosity for discovery).

	$\mathcal{L}$ for 5σ discovery in 2l-SF		
Model	$2l$-SF-A	$2l$-SF-B	$2l$-SF-C
i.	545	623	696
ii.	315	306	273
iii.	181	271	238
iv.	640	843	934
v.	1410	1460	1690
vi.	1090	1610	1500
vii.	944	1450	1510
viii.	732	1090	1190
ix.	360	487	624
xi.	224	450	547

Table 21: Analysis of the discovery potential for supersymmetry for the parameter space of Table 3, using the 2 lepton same flavor (SF) selection criteria of Table 18, where the minimum integrated luminosity needed for 5σ discovery is given in fb^{-1}. The different flavor (DF) signal regions are omitted due to poor performance (i.e. requiring over 3000 fb^{-1} of integrated luminosity for discovery). Model (x) is not listed because the minimum integrated luminosity needed for 5σ discovery exceeded 3000 fb^{-1}

Model	Leading SR	$\mathcal{L}$ (fb^{-1})	Model	Leading SR	$\mathcal{L}$ (fb^{-1})
a.	2l-SF-A	187	i.	2l-SF-A	454
b.	2l-SF-A	362	ii.	2l-SF-C	273
c.	2l-SF-A	165	iii.	2l-SF-A	181
d.	2l-SF-A	781	iv.	2l-SF-A	640
e.	2l-SF-A	1480	v.	2l-SF-A	1410
f.	2l-SF-A	1110	vi.	2l-SF-A	1090
g.	2l-SF-C	1790	vii.	2l-SF-A	944
h.	2l-SF-C	1660	viii.	2l-SF-A	732
j.	2l-SF-C	1880	ix.	2l-SF-A	360
k.	2l-SF-A	97	x.	2l-SF-C	··
			xi.	2l-SF-A	224

Table 22: Integrated luminosity for SUSY production in the leading and sub-leading leptonic (e and μ) signal regions of Tables 18 and 19 for the benchmark points of Tables 1 and 3.

Model	Leading SR	$\mathcal{L}$ (fb^{-1})	Sub-leading SR	$\mathcal{L}$ (fb^{-1})
k.	2l-SF-A	97	2l-SF-B	185
c.	2l-SF-A	165	2l-SF-C	169
a.	2l-SF-A	187	2l-SF-B	266
b.	2l-SF-A	362	1τ-SC2-C	416
d.	2l-SF-A	781	2l-SF-C	884
f.	2l-SF-A	1110	2l-SF-C	1250
e.	2l-SF-A	1480	2l-SF-B	1630
g.	2l-SF-C	1790	2l-SF-A	1850
h.	2l-SF-C	1660	2l-SF-A	1860
j.	2l-SF-C	1880	2l-SF-A	2160

Table 23: The overall minimum integrated luminosities needed for 5σ discovery using the leading and the sub-leading signal regions for stau coannihilation models of Table 1, including the τ based signal regions discussed in Section 4.1 as well as the e and μ based signal regions discussed in Section 4.2.

Model	Leading SR	$\mathcal{L}$ (fb^{-1})	Sub-leading SR	$\mathcal{L}$ (fb^{-1})	Sub-leading **leptonic** SR	$\mathcal{L}$ (fb^{-1})
xi.	2τ-SC2-A	73	2τ-SC2-B	89	2l-SF-A	224
iii.	2l-SF-A	181	2τ-SC2-A	200	2l-SF-C	238
ii.	2l-SF-C	273	2l-SF-B	306	2l-SF-B	306
ix.	2l-SF-A	360	2l-SF-B	487	2l-SF-B	487
v.	1τ-SC1-C	411	1τ-SC1-B	475	2l-SF-A	1410
i.	2τ-SC2-A	477	2l-SF-A	545	2l-SF-A	454
vii.	1τ-SC1-C	508	1τ-SC1-B	605	2l-SF-A	944
iv.	1τ-SC1-C	532	1τ-SC1-B	575	2l-SF-A	640
vi.	1τ-SC1-C	650	1τ-SC2-C	693	2l-SF-A	1090
viii.	1τ-SC1-C	660	2l-SF-A	732	2l-SF-A	732
x.	1τ-SC1-C	1090	1τ-SC1-B	1230	..	..

Table 24: The overall minimum integrated luminosities needed for 5σ discovery using the leading and sub-leading signal regions for the multiparticle coannihilation models of Table 3, including the τ based signal regions discussed in Section 4.1 as well as the e and μ based signal regions discussed in Section 4.2.

Model	$\sigma^{\rm SI}_{p,\chi_1^0} \times 10^{48}$	$\sigma^{\rm SD}_{p,\chi_1^0} \times 10^{46}$	Model	$\sigma^{\rm SI}_{p,\chi_1^0} \times 10^{48}$	$\sigma^{\rm SD}_{p,\chi_1^0} \times 10^{45}$
a.	0.92	4.77	i.	1.33	3.02
b.	0.80	3.67	ii.	1.97	3.54
c.	1.08	5.60	iii.	0.94	1.03
d.	0.80	6.35	iv.	1.94	2.87
e.	0.58	4.43	v.	1.74	2.45
f.	0.64	4.82	vi.	2.90	5.66
g.	0.40	2.39	vii.	1.46	1.93
h.	0.27	1.03	viii.	2.02	3.28
j.	0.53	3.52	ix.	0.96	1.88
k.	1.22	0.25	x.	3.01	4.77
			xi.	1.11	1.53

Table 25: Three left columns: Proton–neutralino spin-independent ($\sigma^{\rm SI}_{p,\chi_1^0}$) and spin-dependent ($\sigma^{\rm SD}_{p,\chi_1^0}$) cross-sections in units of cm^{-2} for the 10 benchmark points of Table 1. Three right columns: Proton–neutralino spin-independent ($\sigma^{\rm SI}_{p,\chi_1^0}$) and spin-dependent ($\sigma^{\rm SD}_{p,\chi_1^0}$) cross-sections in units of cm^{-2} for the 11 benchmark points of Table 3.

7 Figures

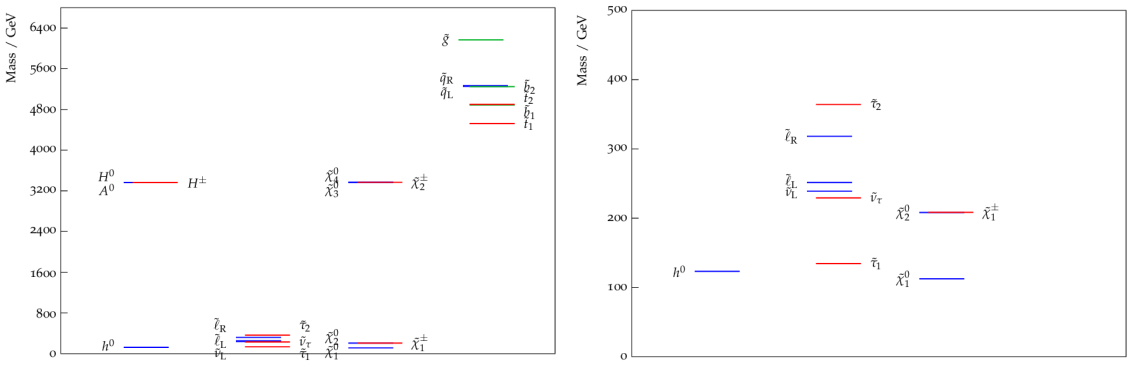

Figure 1: An exhibition of the sparticle mass hierarchy for stau coannihilation model (a). Left panel: Full spectrum. Right panel: Only sparticles with mass < 500 GeV.

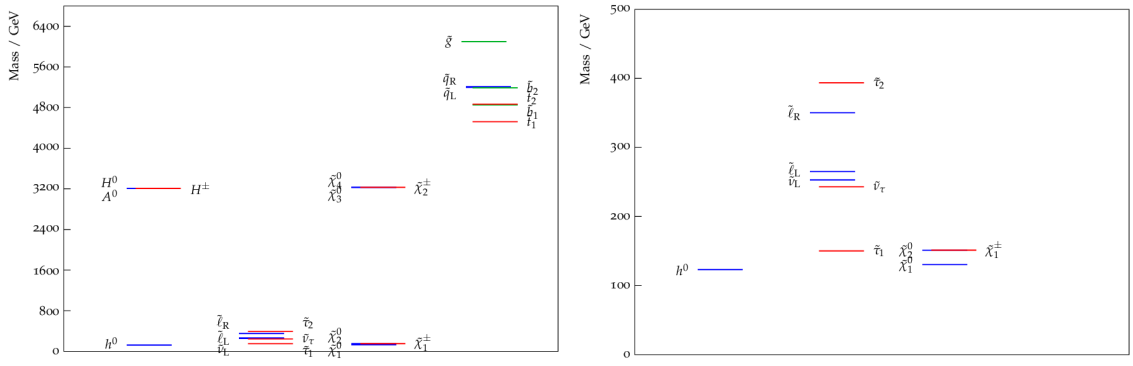

Figure 2: An exhibition of the sparticle mass hierarchy for multiparticle coannihilation model (iii). Left panel: Full spectrum. Right panel: Only sparticles with mass < 500 GeV.

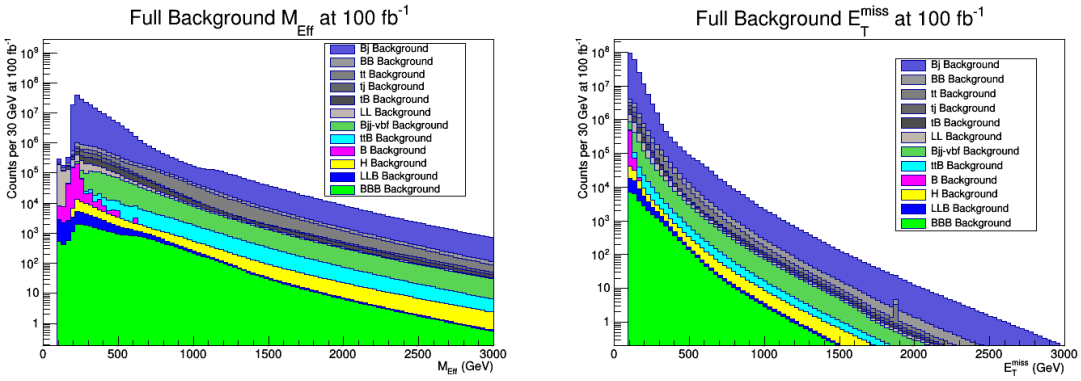

Figure 3: Full SNOWMASS standard model background [54] after triggering cuts and a cut of $E_T^{\rm miss} \geq 100$ GeV, broken into final states and scaled to 100 fb^{-1}. The top panel gives $M_{\rm eff}$(incl.) and the bottom panel gives $E_T^{\rm miss}$. Individual data sets are labeled according to Eq. 1.

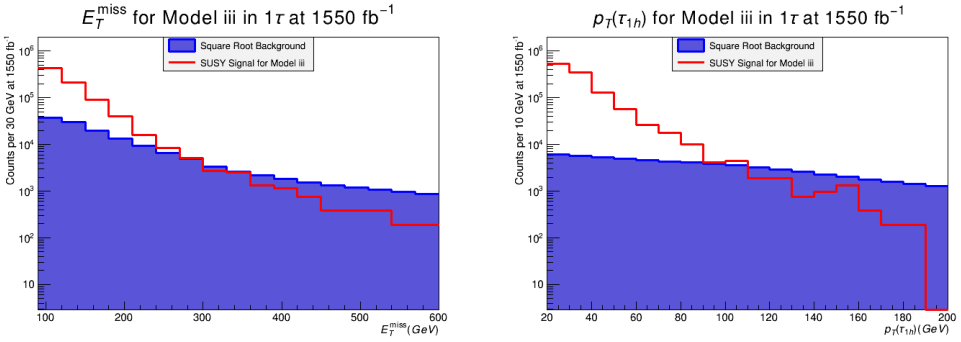

Figure 4: Left panel: Distribution in $E_T^{\rm miss}$ for the 1τ signal region for multiparticle coannihilation model (iii) prior to any cuts. Plotted is the number of counts for the SUSY signal per 30 GeV and the square root of the total SM SNOWMASS background. The analysis is done at 1550 fb^{-1} of integrated luminosity, which gives a 5σ discovery in this signal region. Right panel: The same analysis as in the left panel but for $p_T(\tau_h)$ with counts per 10 GeV.

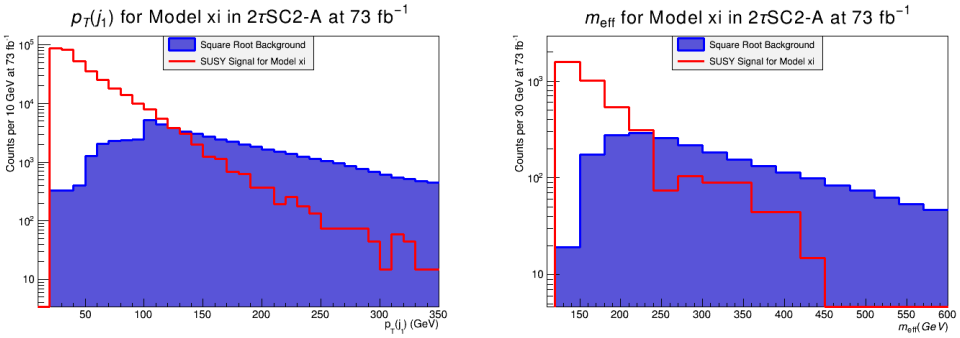

Figure 5: Left panel: Distribution in $p_T(j_1)$ for the 2τSC2-A signal region for multiparticle coannihilation model (xi) prior to any cuts. Plotted is the number of counts for the SUSY signal per 10 GeV and the square root of the total SM SNOWMASS backgrounds. The analysis is done at 73 fb^{-1} of integrated luminosity, which gives a 5σ discovery in this signal region. Right panel: The same analysis as in the left panel but for m_{eff} with counts for the SUSY signal per 30 GeV.

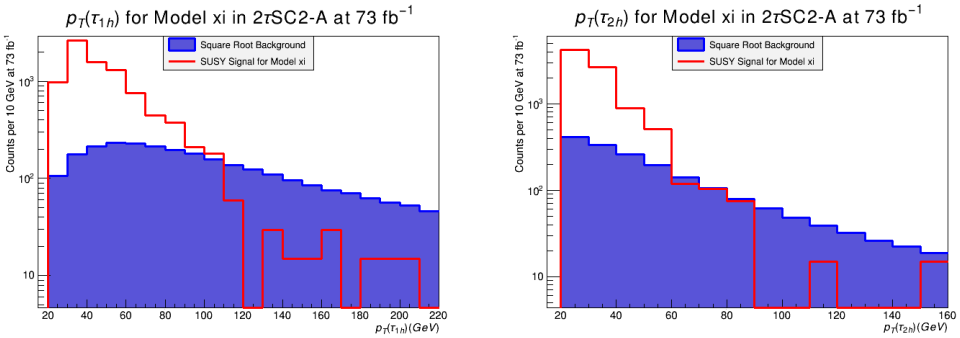

Figure 6: Left panel: Distribution in $p_T(\tau_{1h})$ for the 2τSC2-A signal region for the multiparticle coannihilation model (xi) prior to any cuts. Plotted is the number of counts for the SUSY signal per 10 GeV and the square root of the total SM SNOWMASS backgrounds. The analysis is done at 73 fb^{-1} of integrated luminosity, which gives a 5σ discovery in this signal region. Right panel: The same analysis as in the left panel but for $p_T(\tau_{2h})$.

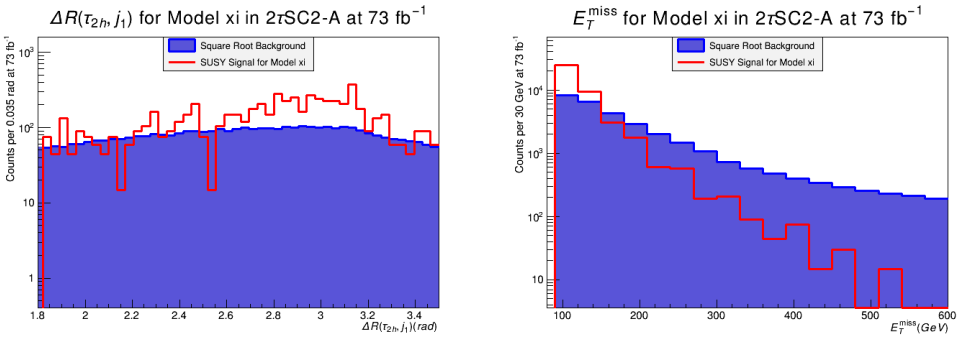

Figure 7: Left panel: Distribution in $\Delta R(\tau_{2h}, j_1)$ for the 2τSC2-A signal region for the multiparticle coannihilation model (xi) prior to any cuts. Plotted is the number of counts for the SUSY signal per 0.035 rad and the square root of the total SM SNOWMASS backgrounds. The analysis is done at 73 fb^{-1} of integrated luminosity, which gives a 5σ discovery in this signal region. Right panel: The same analysis as in the left panel but for E_T^{miss} with counts for the SUSY signal per 30 GeV.

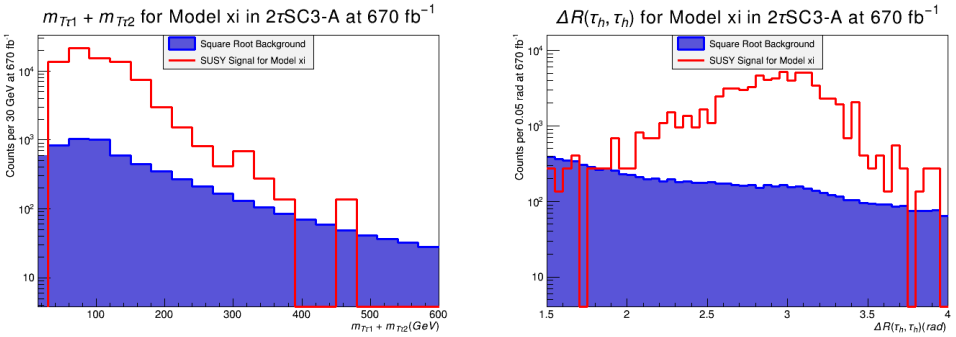

Figure 8: Left panel: Distribution in $m_{T\tau1}+m_{T\tau2}$ for the 2τSC3-A signal region for the multiparticle coannihilation model (xi) prior to any cuts. Plotted is the number of counts for the SUSY signal per 30 GeV and the square root of the total SM SNOWMASS backgrounds. The analysis is done at 670 fb^{-1} of integrated luminosity, which gives a 5σ discovery in this signal region. Right panel: The same analysis as in the left panel but for $\Delta R(\tau_h, \tau_h)$ with counts for the SUSY signal per 0.05 rad.

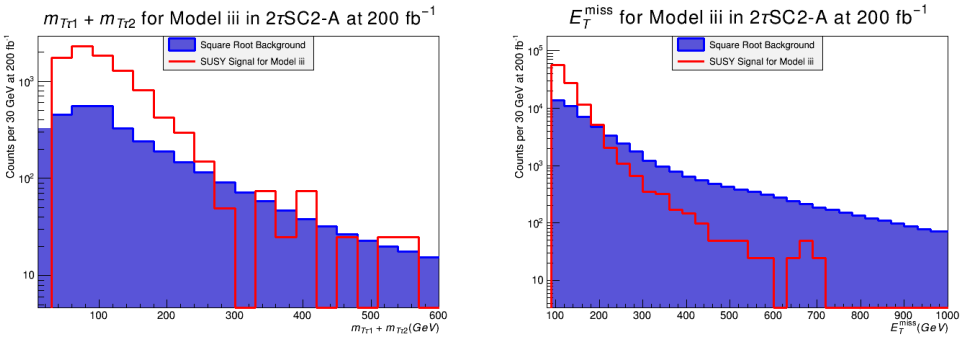

Figure 9: Left panel: Distribution in $m_{T\tau1}+m_{T\tau2}$ for the 2τSC2-A signal region for the multiparticle coannihilation model (iii) prior to any cuts. Plotted is the number of counts for the SUSY signal per 30 GeV and the square root of the total SM SNOWMASS backgrounds. The analysis is done at 200 fb^{-1} of integrated luminosity, which gives a 5σ discovery in this signal region. Right panel: The same analysis as in the left panel but for $E_T^{\rm miss}$ with counts for the SUSY signal per 30 GeV.

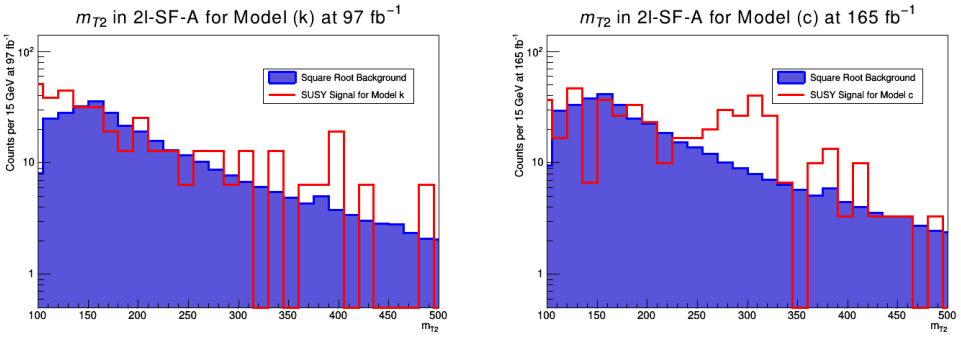

Figure 10: Left panel: Distribution in m_{T2} for the 2l-SF-A signal region defined in Table 18 for stau coannihilation model (k) after cuts in that region. Plotted is the number of counts for the SUSY signal per 15 GeV and the square root of the total standard model SNOWMASS background. The analysis is done at 97 fb^{-1} of integrated luminosity, which gives a 5σ discovery in this signal region. Right panel: The same analysis as in the left panel but for model (c) at 165 fb^{-1}.

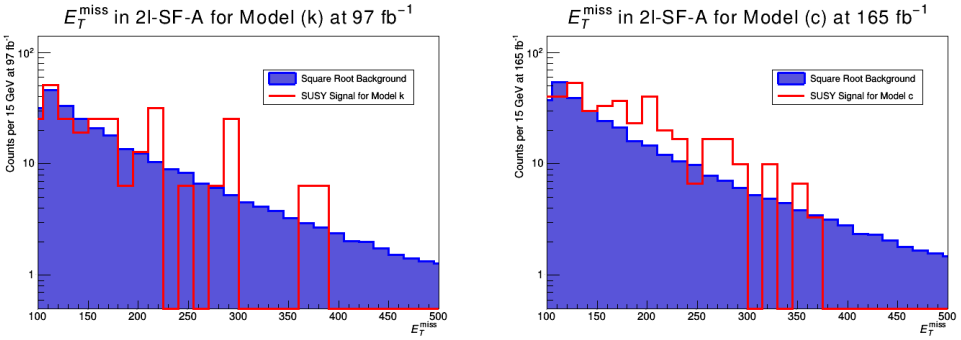

Figure 11: Left panel: Distribution in E_T^{miss} for the 2l-SF-A signal region defined in Table 18 for stau coannihilation model (k) after cuts in that region. Plotted is the number of counts for the SUSY signal per 15 GeV and the square root of the total standard model SNOWMASS background. The analysis is done at 97 fb^{-1} of integrated luminosity, which gives a 5σ discovery in this signal region. Right panel: The same analysis as in the left panel but for model (c) at 165 fb^{-1}.

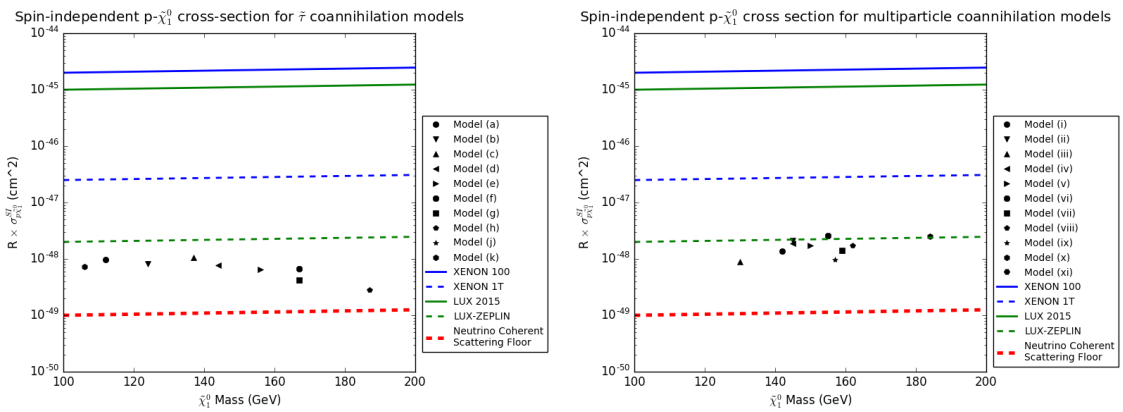

Figure 12: $R \times \sigma^{\rm SI}_{p,\chi_1^0}$ ($R = \rho_{\tilde{\chi}_1^0}/\rho_c$) for models of Tables 1 (left panel) and Table 3 (right panel) as a function of LSP mass displayed alongside the current and projected range of the XENON and LUX experiments and the neutrino floor.

References

[1] F. Englert and R. Brout, Phys. Rev. Lett. **13**, 321 (1964). doi:10.1103/PhysRevLett.13.321

[2] P. W. Higgs, Phys. Rev. Lett. **13**, 508 (1964). doi:10.1103/PhysRevLett.13.508

[3] G. S. Guralnik, C. R. Hagen and T. W. B. Kibble, Phys. Rev. Lett. **13**, 585 (1964). doi:10.1103/PhysRevLett.13.585

[4] S. Chatrchyan *et al.* [CMS Collaboration], Phys. Lett. B **716**, 30 (2012) doi:10.1016/j.physletb.2012.08.021 [arXiv:1207.7235 [hep-ex]].

[5] G. Aad *et al.* [ATLAS Collaboration], Phys. Lett. B **716**, 1 (2012) doi:10.1016/j.physletb.2012.08.020 [arXiv:1207.7214 [hep-ex]].

[6] P. Nath, Annalen Phys. **528**, 167 (2016) doi:10.1002/andp.201500005 [arXiv:1501.01679 [hep-ph]].

[7] A. H. Chamseddine, R. Arnowitt and P. Nath, Phys. Rev. Lett. **49** (1982) 970; P. Nath, R. L. Arnowitt and A. H. Chamseddine, Nucl. Phys. B **227**, 121 (1983); L. J. Hall, J. D. Lykken and S. Weinberg, Phys. Rev. D **27**, 2359 (1983). doi:10.1103/PhysRevD.27.2359

[8] P. Nath, "Supersymmetry, Supergravity, and Unification", Cambridge University Press. ISBN: 9780521197021 (2016).

[9] S. Akula, B. Altunkaynak, D. Feldman, P. Nath and G. Peim, Phys. Rev. D **85**, 075001 (2012) doi:10.1103/PhysRevD.85.075001 [arXiv:1112.3645 [hep-ph]].

[10] A. Arbey, M. Battaglia, A. Djouadi and F. Mahmoudi, JHEP **1209**, 107 (2012) doi:10.1007/JHEP09(2012)107 [arXiv:1207.1348 [hep-ph]].

[11] H. Baer, V. Barger and A. Mustafayev, Phys. Rev. D **85**, 075010 (2012) doi:10.1103/PhysRevD.85.075010 [arXiv:1112.3017 [hep-ph]]; A. Arbey, M. Battaglia, A. Djouadi, F. Mahmoudi and J. Quevillon, Phys. Lett. B **708**, 162 (2012)

doi:10.1016/j.physletb.2012.01.053 [arXiv:1112.3028 [hep-ph]]; P. Draper, P. Meade, M. Reece and D. Shih, Phys. Rev. D **85**, 095007 (2012) doi:10.1103/PhysRevD.85.095007 [arXiv:1112.3068 [hep-ph]]. M. Carena, S. Gori, N. R. Shah and C. E. M. Wagner, JHEP **1203**, 014 (2012) doi:10.1007/JHEP03(2012)014 [arXiv:1112.3336 [hep-ph]]; O. Buchmueller *et al.*, Eur. Phys. J. C **72**, 2020 (2012) doi:10.1140/epjc/s10052-012-2020-3 [arXiv:1112.3564 [hep-ph]]; S. Akula, P. Nath and G. Peim, Phys. Lett. B **717**, 188 (2012) doi:10.1016/j.physletb.2012.09.007 [arXiv:1207.1839 [hep-ph]]. C. Strege, G. Bertone, F. Feroz, M. Fornasa, R. Ruiz de Austri and R. Trotta, JCAP **1304**, 013 (2013) doi:10.1088/1475-7516/2013/04/013 [arXiv:1212.2636 [hep-ph]].

[12] H. Baer, V. Barger and M. Savoy, Phys. Scripta **90**, 068003 (2015) doi:10.1088/0031-8949/90/6/068003 [arXiv:1502.04127 [hep-ph]].

[13] R. L. Arnowitt and P. Nath, Phys. Rev. Lett. **69**, 725 (1992). doi:10.1103/PhysRevLett.69.725

[14] K. Griest and D. Seckel, Phys. Rev. D **43**, 3191 (1991). doi:10.1103/PhysRevD.43.3191

[15] D. Feldman, Z. Liu and P. Nath, Phys. Rev. Lett. **99**, 251802 (2007) Erratum: [Phys. Rev. Lett. **100**, 069902 (2008)] doi:10.1103/PhysRevLett.99.251802 [arXiv:0707.1873 [hep-ph]]; Phys. Lett. B **662**, 190 (2008); JHEP **0804**, 054 (2008); N. Chen, D. Feldman, Z. Liu, P. Nath and G. Peim, Phys. Rev. D **83**, 035005 (2011) doi:10.1103/PhysRevD.83.035005 [arXiv:1011.1246 [hep-ph]]; D. Francescone, S. Akula, B. Altunkaynak and P. Nath, JHEP **1501**, 158 (2015) doi:10.1007/JHEP01(2015)158 [arXiv:1410.4999 [hep-ph]].

[16] J. R. Ellis, K. Enqvist, D. V. Nanopoulos and K. Tamvakis, Phys. Lett. **155B**, 381 (1985). doi:10.1016/0370-2693(85)91591-6

[17] A. Corsetti and P. Nath, Phys. Rev. D **64**, 125010 (2001); CITATION = PHRVA,D64,125010;U. Chattopadhyay and P. Nath, Phys. Rev. D **65**, 075009 (2002); A. Birkedal-Hansen and B. D. Nelson, Phys. Rev. D **67**, 095006 (2003); U. Chattopadhyay and D. P. Roy, Phys. Rev. D **68**, 033010 (2003); D. G. Cerdeno and C. Munoz, JHEP **0410**, 015 (2004); G. Belanger, F. Boudjema, A. Cottrant, A. Pukhov and A. Semenov, Nucl. Phys. B **706**, 411 (2005); H. Baer, A. Mustafayev, E. K. Park, S. Profumo and X. Tata, JHEP **0604**, 041 (2006); K. Choi and H. P. Nilles JHEP **0704** (2007) 006; I. Gogoladze, R. Khalid, N. Okada and Q. Shafi, arXiv:0811.1187 [hep-ph]; S. Bhattacharya, A. Datta and B. Mukhopadhyaya, Phys. Rev. D **78**, 115018 (2008); M. E. Gomez, S. Lola, P. Naranjo and J. Rodriguez-Quintero, arXiv:0901.4013 [hep-ph]; B. Altunkaynak, P. Grajek, M. Holmes, G. Kane and B. D. Nelson, arXiv:0901.1145 [hep-ph]; U. Chattopadhyay, D. Das and D. P. Roy, arXiv:0902.4568 [hep-ph]; S. Bhattacharya and J. Chakrabortty, arXiv:0903.4196 [hep-ph]; S. P. Martin, arXiv:0903.3568 [hep-ph].

[18] D. Matalliotakis and H. P. Nilles, Nucl. Phys. **B435**, 115(1995); M. Olechowski and S. Pokorski, Phys. Lett. **B344**, 201(1995); N. Polonski and A. Pomerol, Phys. Rev.**D51**, 6532(1995); P. Nath and R. Arnowitt, Phys. Rev. D **56**, 2820 (1997); E. Accomando, R. L. Arnowitt, B. Dutta and Y. Santoso, Nucl. Phys. B **585**, 124 (2000) doi:10.1016/S0550-3213(00)00321-7 [hep-ph/0001019]; J. R. Ellis, K. A. Olive and Y. Santoso, Phys. Lett. B **539**, 107 (2002) [arXiv:hep-ph/0204192]; H. Baer, A. Mustafayev, S. Profumo, A. Belyaev and X. Tata, JHEP **0507**, 065 (2005) [arXiv:hep-ph/0504001]; U. Chattopadhyay and D. Das, arXiv:0809.4065 [hep-ph].

[19] K. L. Chan, U. Chattopadhyay and P. Nath, Phys. Rev. D **58**, 096004 (1998) doi:10.1103/PhysRevD.58.096004 [hep-ph/9710473].

[20] J. L. Feng, K. T. Matchev and T. Moroi, Phys. Rev. Lett. **84**, 2322 (2000) doi:10.1103/PhysRevLett.84.2322 [hep-ph/9908309].

[21] U. Chattopadhyay, A. Corsetti and P. Nath, Phys. Rev. D **68**, 035005 (2003) doi:10.1103/PhysRevD.68.035005 [hep-ph/0303201].

[22] H. Baer, C. Balazs, A. Belyaev, T. Krupovnickas and X. Tata, JHEP **0306**, 054 (2003) doi:10.1088/1126-6708/2003/06/054 [hep-ph/0304303].

[23] D. Feldman, G. Kane, E. Kuflik and R. Lu, Phys. Lett. B **704**, 56 (2011) doi:10.1016/j.physletb.2011.08.063 [arXiv:1105.3765 [hep-ph]].

[24] S. Akula, M. Liu, P. Nath and G. Peim, Phys. Lett. B **709**, 192 (2012) doi:10.1016/j.physletb.2012.01.077 [arXiv:1111.4589 [hep-ph]].

[25] G. G. Ross, K. Schmidt-Hoberg and F. Staub, JHEP **1703**, 021 (2017) doi:10.1007/JHEP03(2017)021 [arXiv:1701.03480 [hep-ph]].

[26] P. Nath and P. Fileviez Perez, Phys. Rept. **441**, 191 (2007) doi:10.1016/j.physrep.2007.02.010 [hep-ph/0601023].

[27] M. Liu and P. Nath, Phys. Rev. D **87**, no. 9, 095012 (2013) doi:10.1103/PhysRevD.87.095012 [arXiv:1303.7472 [hep-ph]].

[28] B. Kaufman, P. Nath, B. D. Nelson and A. B. Spisak, Phys. Rev. D **92**, 095021 (2015) doi:10.1103/PhysRevD.92.095021 [arXiv:1509.02530 [hep-ph]].

[29] P. Nath and A. B. Spisak, Phys. Rev. D **93**, no. 9, 095023 (2016) doi:10.1103/PhysRevD.93.095023 [arXiv:1603.04854 [hep-ph]].

[30] J. Dutta, P. Konar, S. Mondal, B. Mukhopadhyaya and S. K. Rai, JHEP **1601**, 051 (2016) doi:10.1007/JHEP01(2016)051 [arXiv:1511.09284 [hep-ph]].

[31] M. Berggren, A. Cakir, D. Krcker, J. List, I. A. Melzer-Pellmann, B. Safarzadeh Samani, C. Seitz and S. Wayand, Eur. Phys. J. C **76**, no. 4, 183 (2016) doi:10.1140/epjc/s10052-016-3914-2 [arXiv:1508.04383 [hep-ph]].

[32] M. Berggren, arXiv:1611.04450 [hep-ph].

[33] T. J. LeCompte and S. P. Martin, Phys. Rev. D **85**, 035023 (2012) doi:10.1103/PhysRevD.85.035023 [arXiv:1111.6897 [hep-ph]]; Phys. Rev. D **84**, 015004 (2011) doi:10.1103/PhysRevD.84.015004 [arXiv:1105.4304 [hep-ph]].

[34] V. Khachatryan *et al.* [CMS Collaboration], Phys. Rev. Lett. **118**, no. 2, 021802 (2017) doi:10.1103/PhysRevLett.118.021802 [arXiv:1605.09305 [hep-ex]].

[35] V. Khachatryan *et al.* [CMS Collaboration], Phys. Lett. B **767**, 403 (2017) doi:10.1016/j.physletb.2017.02.007 [arXiv:1605.08993 [hep-ex]].

[36] L. Morvaj [ATLAS Collaboration], PoS EPS **-HEP2013**, 050 (2013).

[37] J. R. Ellis, T. Falk and K. A. Olive, Phys. Lett. B **444**, 367 (1998) doi:10.1016/S0370-2693(98)01392-6 [hep-ph/9810360]; J. R. Ellis, T. Falk, K. A. Olive and M. Srednicki, Astropart. Phys. **13**, 181 (2000) Erratum: [Astropart. Phys. **15**, 413 (2001)] doi:10.1016/S0927-6505(99)00104-8 [hep-ph/9905481].

[38] R. L. Arnowitt, B. Dutta, A. Gurrola, T. Kamon, A. Krislock and D. Toback, Phys. Rev. Lett. **100**, 231802 (2008) doi:10.1103/PhysRevLett.100.231802 [arXiv:0802.2968 [hep-ph]]; R. L. Arnowitt, A. Aurisano, B. Dutta, T. Kamon, N. Kolev, P. Simeon, D. A. Toback and P. Wagner, Phys. Lett. B **649**, 73 (2007). doi:10.1016/j.physletb.2007.03.043

[39] J. E. Camargo-Molina, B. O'Leary, W. Porod and F. Staub, JHEP **1312**, 103 (2013) doi:10.1007/JHEP12(2013)103 [arXiv:1309.7212 [hep-ph]]; J. E. Camargo-Molina, B. Garbrecht, B. O'Leary, W. Porod and F. Staub, Phys. Lett. B **737**, 156 (2014) doi:10.1016/j.physletb.2014.08.036 [arXiv:1405.7376 [hep-ph]].

[40] A. Flrez, L. Bravo, A. Gurrola, C. vila, M. Segura, P. Sheldon and W. Johns, Phys. Rev. D **94**, no. 7, 073007 (2016) doi:10.1103/PhysRevD.94.073007 [arXiv:1606.08878 [hep-ph]].

[41] S. Akula and P. Nath, Phys. Rev. D **87**, no. 11, 115022 (2013) doi:10.1103/PhysRevD.87.115022 [arXiv:1304.5526 [hep-ph]].

[42] The ATLAS collaboration [ATLAS Collaboration], ATLAS-CONF-2016-096.

[43] K. Kowalska, L. Roszkowski, E. M. Sessolo and A. J. Williams, JHEP **1506**, 020 (2015) doi:10.1007/JHEP06(2015)020 [arXiv:1503.08219 [hep-ph]].

[44] L. E. Ibanez and G. G. Ross, Comptes Rendus Physique **8**, 1013 (2007) doi:10.1016/j.crhy.2007.02.004 [hep-ph/0702046 [HEP-PH]].

[45] B. C. Allanach, Comput. Phys. Commun. **143**, 305 (2002) doi:10.1016/S0010-4655(01)00460-X [hep-ph/0104145].

[46] B. C. Allanach, S. P. Martin, D. G. Robertson and R. Ruiz de Austri, arXiv:1601.06657 [hep-ph].

[47] G. Blanger, F. Boudjema, A. Pukhov and A. Semenov, Comput. Phys. Commun. **192**, 322 (2015) doi:10.1016/j.cpc.2015.03.003 [arXiv:1407.6129 [hep-ph]].

[48] A. Buckley, Eur. Phys. J. C **75**, no. 10, 467 (2015) doi:10.1140/epjc/s10052-015-3638-8 [arXiv:1305.4194 [hep-ph]].

[49] J. Alwall *et al.*, JHEP **1407**, 079 (2014) doi:10.1007/JHEP07(2014)079 [arXiv:1405.0301 [hep-ph]].

[50] A. Djouadi, M. M. Muhlleitner and M. Spira, Acta Phys. Polon. B **38**, 635 (2007) [hep-ph/0609292].

[51] T. Sjostrand, S. Mrenna and P. Z. Skands, JHEP **0605**, 026 (2006) doi:10.1088/1126-6708/2006/05/026 [hep-ph/0603175].

[52] S. Ovyn, X. Rouby and V. Lemaitre, arXiv:0903.2225 [hep-ph].

[53] R. Brun and F. Rademakers, Nucl. Instrum. Meth. A **389**, 81 (1997). doi:10.1016/S0168-9002(97)00048-X

[54] A. Avetisyan *et al.*, arXiv:1308.1636 [hep-ex].

[55] C. G. Lester and D. J. Summers, Phys. Lett. B **463**, 99 (1999) doi:10.1016/S0370-2693(99)00945-4 [hep-ph/9906349].

[56] A. Barr, C. Lester and P. Stephens, J. Phys. G **29**, 2343 (2003) doi:10.1088/0954-3899/29/10/304 [hep-ph/0304226].

[57] C. G. Lester and B. Nachman, JHEP **1503**, 100 (2015) doi:10.1007/JHEP03(2015)100 [arXiv:1411.4312 [hep-ph]].

[58] `https://twiki.cern.ch/twiki/bin/view/CMSPublic/LumiPublicResults#2016_Proton_Proton_13_TeV_Collis`
`http://lpc.web.cern.ch/cgi-bin/plots.py`

[59] `https://twiki.cern.ch/twiki/bin/view/AtlasPublic/LuminosityPublicResultsRun2#Publications_and_Conference_Resu`

[60] D. Feldman, Z. Liu, P. Nath and G. Peim, Phys. Rev. D **81**, 095017 (2010) doi:10.1103/PhysRevD.81.095017 [arXiv:1004.0649 [hep-ph]].

[61] L. Hui, J. P. Ostriker, S. Tremaine and E. Witten, Phys. Rev. D **95**, no. 4, 043541 (2017) doi:10.1103/PhysRevD.95.043541 [arXiv:1610.08297 [astro-ph.CO]].

[62] D. J. E. Marsh, Phys. Rept. **643**, 1 (2016) doi:10.1016/j.physrep.2016.06.005 [arXiv:1510.07633 [astro-ph.CO]].

[63] J. Halverson, C. Long and P. Nath, arXiv:1703.07779 [hep-ph].

[64] G. Aad *et al.* [ATLAS Collaboration], Eur. Phys. J. C **76**, no. 11, 581 (2016) doi:10.1140/epjc/s10052-016-4395-z [arXiv:1510.03823 [hep-ex]].

[65] D. Larson *et al.*, Astrophys. J. Suppl. **192**, 16 (2011) doi:10.1088/0067-0049/192/2/16 [arXiv:1001.4635 [astro-ph.CO]].

[66] P. A. R. Ade *et al.* [Planck Collaboration], Astron. Astrophys. **594**, A13 (2016) doi:10.1051/0004-6361/201525830 [arXiv:1502.01589 [astro-ph.CO]].

[67] L. E. Strigari, New J. Phys. **11**, 105011 (2009) doi:10.1088/1367-2630/11/10/105011 [arXiv:0903.3630 [astro-ph.CO]].

[68] M. Schumann, EPJ Web Conf. **96**, 01027 (2015) doi:10.1051/epjconf/20159601027 [arXiv:1501.01200 [astro-ph.CO]].

[69] P. Cushman *et al.*, arXiv:1310.8327 [hep-ex].